癌組織では正常組織よりも低 pH であることから，PVD を薬物キャリアとして適用した場合，病態組織でのみ効果的に蛋白質が pH 応答的に徐放されることを意味している．この PVD をマウスに尾静脈内投与したところ，数時間後に投与量の約 80% が腎臓へ選択的に集積し，4 日後には 40% に減少していた（Fig. 7）．この PVD は腎尿細管上皮細胞へのみ選択的に取り込まれるが，細胞毒性を全く示さないうえ，大量投与しても腎臓を含め他の組織に何ら傷害を及ぼさない．さらに PVD でバイオコンジュゲーションした抗炎症蛋白質（SOD）は生体内安定性に優れ，かつ静脈内投与後，選択的に腎臓へ高集積し，著しい腎炎治療作用を発揮することを見出した．高齢化社会を迎え，腎不全を初めとする腎疾患が世界的に深刻な社会問題となっている．[38] しかし慢性腎疾患に対する治療は，腎移植と透析に頼らざるを得ないのが現状であり，患者の QOL（Quality of Life）の観点からも，安全かつ有効な薬物療法の確立が待望されている．[39] 本観点から現在，上述した「医薬価値に優れた機能性人工蛋白質を迅速創製できる蛋白質分子進化戦略」による機能性人工蛋白質の創製や部位特異的バイオコンジュゲーション

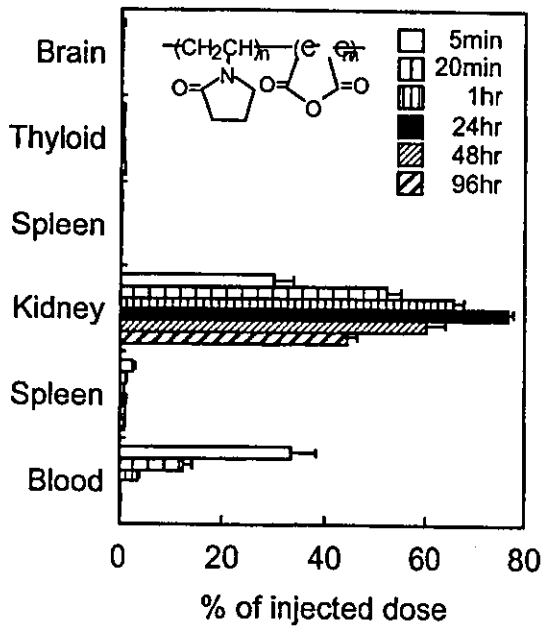

Fig. 7. Tissue Distribution of Poly (VP-co-DMMAn); PVD after *i.v.* Injection

^{125}I-labelled PVD was injected into the tail vein of BALB/c mice and tissues were collected over different periods of time post-injection (from 5 mins to 96 hrs) and the radioactivity measured by γ-counter. Each point represents the mean ±S.D.

システムとの融合により，新たな腎疾患治療戦略の確立をさらに推進している．

6. おわりに

本稿で紹介した 3 段階の「プロテオーム創薬に叶う DDS 基盤テクノロジー」は，プロテオーム創薬の実現に向けて，相乗的に機能するものと期待している．一方で最近，Gene shuffling[40] や人工遺伝暗号システム[41] などを用いた機能性人工蛋白質の創出に注目が集まっている．これら興味深いアプローチは天然に存在しない新たなアミノ酸配列を有した人工蛋白質を作製しようとするものであるが，残念ながら臨床応用可能な非天然型生理活性蛋白質の創製には至っていない．当然のことながら，本研究で確立した DDS 基盤テクノロジーはこれら非天然型生理活性蛋白質の探索や創製，安定化や高機能化にも適用可能であり，現在 Gene shuffling 法とファージ表面提示法を融合した新たな機能性人工蛋白質の創出システムの構築を進めている．

また前述したように疾患プロテオミクス情報を有効活用したプロテオーム創薬を推進するためにはまず，多種多様な蛋白質とその構造変異体を網羅的に作製し，これらのレセプター・リガンド結合の様式・強度などをも含めた機能情報をハイスループットに評価可能な方法論の構築と，その立体構造との連関を網羅的に評価することが必須となる．そのうえで，ゲノムシーケンス情報を基に新たに見出された蛋白性シーズなどの機能と構造を予測し得るバイオインフォマティクスが構築されて，ようやく真の意味でプロテオーム創薬が可能となってくる．この点，ファージ表面提示法を駆使した「医薬価値に優れた機能性人工蛋白質を迅速創製できる蛋白質的分子進化戦略」は，膨大な多様性を持った構造変異体を創出し，その機能解析を迅速に大量解析し得る最適の基盤テクノロジーとなり得る．以上の研究成果は，得られた数多くの機能性人工蛋白質の立体構造と機能特性との連関評価を通じて，「機能（医薬価値）→構造」に関する知見の集積が可能となり，将来的に機能性人工蛋白質を合理的設計し得る「プロテオーム創薬のためのバイオインフォマティクス」の構築にも貢献し得るものと期待される．

謝辞　筆者が平成 16 年度日本薬学会奨励賞を受賞できましたのは，ひとえに神戸学院大学学長・

大阪大学名誉教授の恩師　真弓忠範先生のご懇篤なるご指導，ご鞭撻の賜であり，心から厚く御礼を申し上げます．また本総説で示した筆者のこれまでの研究は，主として大阪大学薬学研究科助教授，中川晋作先生をはじめとする大阪大学薬学研究科薬剤学分野の皆様にご協力を頂きました．この場をお借りして感謝申し上げます．最後になりましたが，本研究は文部科学省科学研究費，厚生労働省科学研究費に加え，ヒューマンサイエンス振興財団や武田科学振興財団，千里ライフサイエンス振興財団のご援助を賜りました．ここに御礼を申し上げます．

REFERENCES AND NOTES

1) Present address: National Institute of Health Sciences, Osaka Branch Fundamental Research Laboratories for Development of Medicine, 7-6-8 Saito-Asagi, Ibaraki 567-0085, Japan.
2) Yamamoto Y., Tsutsumi Y., Yoshioka Y., Nishibata T., Kobayashi K., Okamoto T., Mukai Y., Shimizu T., Nakagawa S., Nagata S., Mayumi T., *Nat. Biotechnol.*, **21**, 546–552 (2003).
3) Tsutsumi Y., Onda M., Nagata S., Lee B., Kreitman R. J., *Proc. Natl. Acad. Sci. U.S.A.*, **97**, 8548–8553 (2000).
4) Kamada H., Tsutsumi Y., Sato-Kamada K., Yamamoto Y., Yoshioka Y., Okamoto T., Nakagawa S., Nagata S., *Nat. Biotechnol.*, **21**, 399–404 (2003).
5) Onda M., Nagata S., Tsutsumi Y., Vincent J. J., Wang Q., Kreitman R. J., Lee B., *Cancer Res.*, **61**, 5070–5077 (2001).
6) Smith G. P., *Science*, **228**, 1315–1317 (1985).
7) Oettgen H. F., Carswell E. A., Kassel R. L., Fiore N., Williamson B., Hoffmann M. K., Haranaka K., *Recent Results Cancer Res.*, **75**, 207–212 (1980).
8) Aggarwal B. B., Kohr W. J., Hass P. E., Moffat B., Spencer S. A., Henzel W. J., Bringman T. S., Nedwin G. E., Goeddel D. V., *J. Biol. Chem.*, **260**, 2345–2354 (1985).
9) Jones E. Y., Stuart D. I., *Nature*, **338**, 225–228 (1989).
10) Old L. J., *Science*, **230**, 630–632 (1985).
11) Sugarman B. J., Aggarwal B. B., Hass P. E., Figari I. S., Palladino Jr. M. A., Shepard H. M., *Science*, **230**, 943–945 (1985).
12) Creaven P. J., Brenner D. E., Cowens J. W., Huben R. P., Wolf R. M., Takita H., Arbuck S. G., Razack M. S., Proefrock A. D., *Cancer Chemother. Pharmacol.*, **23**, 186–191 (1989).
13) Chapman P. B., Lester T. J., Casper E. S., Gabrilove J. L., Wong G. Y., Kempin S. J., Gold P. J., Welt S., Warren R. S., Starnes H. F., *J. Clin. Oncol.*, **5**, 1942–1951 (1987).
14) Kimura K., Taguchi T., Urushizaki I., Ohno R., Abe O., Furue H., Hattori T., Ichihashi H., Inoguchi K., Majima H., *Cancer Chemother. Pharmacol.*, **20**, 223–229 (1987).
15) Spriggs D. R., Sherman M. L., Michie H., Arthur K. A., Imamura K., Wilmore D., Frei E. 3rd, Kufe D. W., *J. Natl. Cancer Inst.*, **80**, 1039–1044 (1988).
16) Yoshida J., Wakabayashi T., Mizuno M., Sugita K., Yoshida T., Hori S., Mori T., Sato T., Karashima A., Kurisu K., J. *Neurosurg.*, **77**, 78–83 (1992).
17) Taguchi T., *Gan To Kagaku Ryoho*, **13**, 3491–3497 (1986).
18) Eggermont A. M., Schraffordt Koops H., Lienard D., Kroon B. B., van Geel A. N., Hoekstra H. J., Lejeune F. J., *J. Clin. Oncol.*, **14**, 2653–2665 (1996).
19) Halme M., Maasilta P., Repo H., Leirisalo-Repo M., Taskinen E., Mattson K., Cantell K., *J. Immunother. Emphasis Tumor Immunol.*, **15**, 283–291 (1994).
20) Anasetti C., Hansen J. A., Waldmann T. A., Appelbaum F. R., Davis J., Deeg H. J., Doney K., Martin P. J., Nash R., Storb R., *Blood*, **84**, 1320–1327 (1994).
21) Vaglini M., Belli F., Santinami M., Arienti F., Parmiani G., Persiani L., Santoro N., Grazia Inglese M., D'Elia F., Cascinelli N., *Ann. Surg. Oncol.*, **2**, 61–70 (1995).
22) Debs R. J., Fuchs H. J., Philip R., Brunette E. N., Duzgunes N., Shellito J. E., Liggitt D., Patton J. R., *Cancer Res.*, **50**, 375–380 (1990).
23) Okada N., Kaneda Y., Miyamoto H., Yamamoto Y., Mizuguchi H., Tsutsumi Y., Nakagawa S., Mayumi T., *Jpn. J. Cancer Res.*, **87**, 831–836 (1996).
24) Utoguchi N., Mizuguchi H., Saeki K., Ikeda K., Tsutsumi Y., Nakagawa S., Mayumi T.,

Cancer Lett., **89**, 7–14 (1995).
25) Utoguchi N., Mizuguchi H., Dantakean A., Makimoto H., Wakai Y., Tsutsumi Y., Nakagawa S., Mayumi T., *Br. J. Cancer*, **73**, 24–28 (1996).
26) Kayton M. L., Libutti S. K., *Curr. Opin. Investig. Drugs*, **2**, 136–138 (2001).
27) Gaskill H. V. 3rd, *J. Surg. Res.*, **44**, 664–671 (1988).
28) Tsan M. F., White J. E., Santana T. A., Lee C. Y., *J. Appl. Physiol.*, **68**, 1211–1219 (1990).
29) Kamada H., Tsutsumi Y., Yamamoto Y., Kihira T., Kaneda Y., Mu Y., Kodaira H., Tsunoda S. I., Nakagawa S., Mayumi T., *Cancer Res.*, **60**, 6416–6420 (2000).
30) Kaneda Y., Yamamoto Y., Kamada H., Tsunoda S., Tsutsumi Y., Hirano T., Mayumi T., *Cancer Res.*, **58**, 290–295 (1998).
31) Tsutsumi Y., Tsunoda S., Kamada H., Kihira T., Kaneda Y., Ohsugi Y., Mayumi T. *Thromb. Haemost.*, **77**, 168–173 (1997).
32) Tsutsumi Y., Kihira T., Tsunoda S., Kanamori T., Nakagawa S., Mayumi T., *Br. J. Cancer*, **71**, 963–968 (1995).
33) Tsutsumi Y., Tsunoda S., Kamada H., Kihira T., Nakagawa S., Kaneda Y., Kanamori T., Mayumi T., *Br. J. Cancer*, **74**, 1090–1095 (1996).
34) Tsutsumi Y., Kihira T., Tsunoda S., Kamada H., Nakagawa S., Kaneda Y., Kanamori T., Mayumi T., *J. Pharmacol. Exp. Ther.*, **278**, 1006–1011 (1996).
35) Yamagishi J., Kawashima H., Matsuo N., Ohue M., Yamayoshi M., Fukui T., Kotani H., Furuta R., Nakano K., Yamada M., *Protein Eng.*, **3**, 713–719 (1990).
36) Van Ostade X., Tavernier J., Prange T., Fiers W., *EMBO J.*, **10**, 827–836 (1991).
37) Loetscher H., Stueber D., Banner D., Mackay F., Lesslauer W., *J. Biol. Chem.*, **268**, 26350–26357 (1993).
38) Jones C. A., McQuillan G. M., Kusek J. W., Eberhardt M. S., Herman W. H., Coresh J., Salive M., Jones C. P., Agodoa L. Y., *Am. J. Kidney Dis.*, **32**, 992–999 (1998).
39) Progress and Priorities: Renal disease research plan. Peport of the strategic planning conferences-Renal research properties-sponsored by National Institute of Diabetes and Digestive and Kidney Disease, Council of American Kidney Societies, (December 5–6, 1998 & February 4–5, 1999).
40) Chang C. C., Chen T. T., Cox B. W., Dawes G. N., Stemmer W. P., Punnonen J., Patten P. A., *Nat. Biotechnol.*, **17**, 793–797 (1999).
41) Hirao I., Ohtsuki T., Fujiwara T., Mitsui T., Yokogawa T., Okuni T., Nakayama H., Takio K., Yabuki T., Kigawa T., Kodama K., Nishikawa K., Yokoyama S., *Nat. Biotechnol.*, **20**, 177–182 (2002).

Available online at www.sciencedirect.com
SCIENCE DIRECT
Biomaterials 25 (2004) 3259–3266
Biomaterials
www.elsevier.com/locate/biomaterials

The use of PVP as a polymeric carrier to improve the plasma half-life of drugs

Yoshihisa Kaneda[1], Yasuo Tsutsumi*[,1], Yasuo Yoshioka[1], Haruhiko Kamada, Yoko Yamamoto, Hiroshi Kodaira, Shin-ichi Tsunoda, Takayuki Okamoto, Yohei Mukai, Hiroko Shibata, Shinsaku Nakagawa, Tadanori Mayumi

Department of Biopharmaceutics, Graduate School of Pharmaceutical Sciences, Osaka University, 1-6 Yamadaoka, Suita, Osaka 565-0871, Japan

Received 24 June 2003; accepted 29 September 2003

Abstract

To achieve an optimum drug delivery such as targeting or controlled release utilizing bioconjugation with polymeric modifier, the conjugate between drugs and polymeric modifiers must be designed to show desirable pharmacokinetic characteristics in vivo. In this study, we assessed the biopharmaceutical properties of various nonionic water-soluble polymers as polymeric drug carriers. Polyvinylpyrrolidone (PVP) showed the longest mean resident time (MRT) after i.v. injection of all nonionic polymers with the same molecular size. In fact, tumor necrosis factor-α (TNF-α) bioconjugated with PVP (PVP-TNF-α) circulated longer than TNF-α bioconjugated with polyethylene glycol (PEG-TNF-α) with the same molecular size. Each nonionic polymeric modifier showed a different tissue distribution. Dextran was accumulated in the spleen and liver. Polydimethylacrylamide (PDAAm) tended to distribute in the kidney. However, PVP showed the minimum volume of tissue distribution. These results suggested that PVP is the most suitable polymeric modifier for prolonging the circulation lifetime of a drug and localizing the conjugated drug in blood.

Keywords: Polyethylene glycol (PEG); Polyvinylpyrrolidone (PVP); Bioconjugation; Tumor necrosis factor-alpha (TNF-α); Polymeric modifier

1. Introduction

In this post-genome era, the focus on life science research has shifted from genome analyses to genetic and protein function analyses, and recent advances in pharmacoproteomics have been drastic. Due to recent advances in structural genomics, the functions of numerous proteins will be clarified. Thus, the therapeutic application of bioactive proteins, such as newly identified proteins and cytokines, has been highly expected [1–4]. However, most of these proteins are limited in their clinical application because of unexpectedly low therapeutic effects. The reason for this limitation is that these proteins are immediately decomposed by various proteases in vivo, and are rapidly excreted from the blood circulation. Therefore, frequent administration at an excessively high dose is required to reveal their therapeutic effects in vivo. As a result, homeostasis is destroyed, and unexpected side effects occur. Many cancer chemotherapies utilizing anticancer antibiotics are also limited by such problems. Therefore, in order to overcome the weak points peculiar to many proteins, we attempted to perform chemical modification (bioconjugation) with water-soluble polymers [5–9]. Bioconjugation with polymeric modifiers improves the plasma clearance and body distribution, resulting in an increase of therapeutic effects and a decrease of side effects. Our results suggest that investigation of the relationship between degree of modification by polymer, molecular size, and specific activity on cytokine bioconjugation may accomplish an increase of therapeutic effect and a decrease of side effects. In addition, our previous study indicates that optimally bioconjugated drugs can achieve well-balanced tissue transport, receptor binding, and plasma clearance, resulting in a selective increase of therapeutic effects.

On the other hand, in order to deliver a bioconjugated drug to targeted tissue, the conjugate must be designed to show desirable pharmacokinetic characteristics, such

*Corresponding author. Tel.: +81-66879-8178; fax: +81-66879-8178.
E-mail address: tsutsumi@phs.osaka-u.ac.jp (Y. Tsutsumi).
[1]These authors contributed equally to the work.

0142-9612/$ - see front matter © 2003 Elsevier Ltd. All rights reserved.
doi:10.1016/j.biomaterials.2003.10.003

as plasma clearance and tissue distribution. It is well known that the fate and distribution of the conjugates can be attributed to the physicochemical properties of polymeric modifiers, such as molecular weight, electric charge, and hydrophilic–lipophilic balance [10]. The increase of therapeutic effects of drug bioconjugated with polymeric modifier is attributed to the pharmacokinetics of bioconjugated drug. Therefore, selecting the polymeric modifier by considering the influence of physicochemical characteristics on pharmacokinetics of polymeric modifier is markedly important. As mentioned above, sequential and multiple strategies are needed for optimization of drug therapy based on bioconjugation: (i) optimum selection of polymeric modifier considering the disposition of drugs and objectives such as targeting or controlled release; (ii) bioconjugation based on estimation of characterization, such as molecular size, modification site, degree of modification, and specific activity; and (iii) assessment of therapeutic effect and pharmacokinetics of bioconjugated drug.

In the present study, we first focused on nonionic water-soluble polymers and tried to clarify the pharmacokinetic properties of various polymeric modifiers, which could be modified by the physicochemical property, on mice bearing solid tumors. The polymer formulations used to evaluate these are PEG, polyvinylpyrrolidone (PVP), polyacrylamide (PAAm), polydimethylacrylamide (PDAAm), polyvinyl alcohol (PVA), and dextran. PVP, PAAm, and PDAAm could be functionalized by introduction of various comonomers on radical polymerization. PVA and dextran have many primary OH groups that can be used for bioconjugation on the side chain. Each ^{125}I-labeled water-soluble polymer was injected i.v. into tumor-bearing mice, and plasma clearance in the circulation and tissue distribution were measured. Moreover, we assessed the feasibility of polymeric modifiers for drug delivery based on pharmacokinetic analysis.

2. Materials and methods

2.1. Materials

PEGs (average molecular weight: 12,000, 50,000, 70,000, 500,000), acrylamide and *N*,*N*′-dimethylacrylamide, sodium pyrosulfate, chloramine T (sodium *p*-toluenesulfonchloramide trihydrate), thyramine hydrochloride, *N*,*N*′-carbonyldiimidazole, dicyclohexylcarbodiimide, *N*-vinyl-2-pyrrolidone, and *N*-hydroxysuccinimide were purchased from Wako Pure Chemical Industries, Ltd., Osaka, Japan. Methoxypolyethylene glycol-succinimidyl succinate (average molecular weight: 5000) and dextran (average molecular weight: 10,400) were obtained from Sigma Chemical Co., St. Louis, MO. PVA (80% hydrolyzed, average molecular weight: 9000–10,000) and 4,4′-azobis-(4-cyanovaleric acid) (ACVA) were purchased from Aldrich Chemical Company, Inc., Milwaukee, WI. Gel filtration chromatography (GFC) was performed by TSKgel G4000PW and TSKgel-3000 columns purchased from Tosoh Corporation, Tokyo, Japan. Econo-Pac® 10 DG columns were purchased from Bio-rad Laboratories, Hercules CA, USA. 1-Ethyl-3-(3-dimethylaminopropyl)carbodiimide hydrochloride (water-soluble carbodiimide; WSC) and β-mercaptopropionic acid (β-MP) were purchased from Dojindo Laboratories, Kumamoto, Japan. Na^{125}I (3.7 GBq/ml) solution and radioiodination system for lactoperoxidase method was purchased from NEN Research Products, Boston, MA, USA. All other chemicals were commercial reagent-grade products. Natural human tumor necrosis factor-alpha (TNF-α) was generously provided by Hayashibara Biological Laboratories, Okayama, Japan.

2.2. Animals and cells

Male ddY mice (5 weeks old) and female Balb/c mice (5 weeks old) were obtained from SLC, Hamamatsu, Japan. Sarcoma-180 (S-180) was provided from Cancer Cell Repository (CCR), Institute of Development, Aging and Cancer, Tohoku University. Meth-A cells were generously provided by Mochida pharmaceutical Co., Ltd. S-180 cells and Meth-A fibrosarcoma cells were maintained by intraperitoneal injection of cells obtained from ascitic fluid in ddY mice and Balb/c mice respectively.

2.3. Synthesis and purification of water-soluble polymers

PVP was synthesized by the radical polymerization method using ACVA and β-MP as a radical initiator and a chain transfer agent, respectively. *N*-vinylpyrrolidone, ACVA, and β-MP were added to dry *N*,*N*′-dimethylformamide (DMF). The reaction was initiated by incubation at 60°C. After incubation for 6 h, PVP was extracted in diethyl ether. The extracted PVP was dialyzed by distilled water to remove the nonreacted monomer, initiator, and chain transfer agent. PAAm and PDAAm were synthesized in dry methanol. Radical polymerization, extraction and dialysis were carried out as for PVP. PVA, dextran, and the water-soluble polymers synthesized in this study were separated into fractions by GFC in order to obtain a polymer with a narrow molecular-weight distribution. In addition, the number-average molecular weight of each fraction was calculated by comparison with PEG standards, and the same fraction of each polymer (number-average molecular weight: 5000, molecular weight dispersity <1.14) was used.

2.4. Preparation of ^{125}I-labeled polymers

Radiolabeled polymeric modifiers were prepared by the chloramine-T method. PEGs (average molecular weight: 12,000, 50,000, 70,000, 500,000), PVA, and dextran dissolved in 1,4-dioxan were reacted with *N*,*N*′-carbonyldiimidazole for 6 h at room temperature. After dialysis in water, the activated polymers were reacted with a two-fold molar excess of thyramine hydrochloride for 48 h at 4°C. The reaction mixture was dialyzed in water and lyophilized. PAAm and PDAAm were activated with WSC, and reacted with an excessive amount of thyramine hydrochloride for 24 h at 4°C. PVP dissolved in DMF was activated with dicyclohexylcarbodiimide and *N*-hydroxysuccinimide, and reacted with an excessive amount of thyramine hydrochloride for 24 h at 4°C. Methoxypolyethylene glycol-succinimidyl succinate (average molecular weight: 5000) was also reacted with an excessive amount of thyramine hydrochloride for 24 h at 4°C. These reaction mixtures were also dialyzed in water and lyophilized. Polymer-thyramine conjugates dissolved in 0.4 M sodium phosphate buffer (2.5 mg/ml) and Na^{125}I (100 mCi/ml) were mixed in a microcentrifuge tube on ice. The labeling reaction was started by the addition of 3.8 mM chloramine-T. After iodination, the reaction was stopped by the addition of 2.5 mM sodium pyrosulfate. ^{125}I-labeled polymer was purified by GFC on the Econo-Pac® 10 DG column.

2.5. Measurement of plasma clearance and body distribution of ^{125}I-labeled polymer

S-180 cells were implanted intradermally (5×10^5/200 μl/site) into mice. On day 7, when the length of the tumors exceeded 7 mm, the mice were used for experiments. Mice bearing S-180 solid tumors were intravenously injected with ^{125}I-labeled polymer (1×10^6 cpm/200 μl). After injection, blood was collected from the tail vein at indicated times and the radioactivity was measured by a γ-counter. By rechromatographic analysis, we found that almost all the plasma ^{125}I-radioactivity at 3 h after i.v. injection was derived from intact ^{125}I-labeled polymers, but not free ^{125}I. To estimate the tissue distribution, mice were housed in metabolic cages to collect urine and sacrificed 3 h after i.v. injection. Each organ was collected, and the radioactivity was counted. The tissue distribution was expressed by the ratio of tissue radioactivity (tissue-cpm/tissue-mg) to blood radioactivity (blood-cpm/blood-mg). The pharmacokinetic parameters of each polymer were evaluated by curve fitting by means of the nonlinear least-squares program (MULTI) [11]. The peripheral distribution volume (Vd_2), the elimination constant from the central compartment (k_e), total clearance (CL_{tot}), and mean residence time (MRT) were calculated.

2.6. Synthesis of PEG-TNF-α and PVP-TNF-α

Natural human TNF-α in phosphate-buffered saline was allowed to react with a 60-fold molar excess of methoxypolyethylene glycol-succinimidyl succinate at room temperature for 10 min. The reaction was stopped by the addition of five-fold molar excess of ε-amino-n-caproic acid. PEG-TNF-α was separated into several fractions by GFC. PVP-TNF-α was also synthesized and separated in the same way. The number-average molecular weight of native TNF-α, PEG-TNF-α and PVP-TNF-α was estimated by GFC analysis by comparison with protein standards. In order to measure the elimination profile of PEG-TNF-α and PVP-TNF-α in blood, the conjugates with same molecular size (100,000–110,000) were used.

2.7. Measurement of plasma clearance of PEG-TNF-α and PVP-TNF-α

Native TNF-α, PEG-TNF-α and PVP-TNF-α were radiolabeled with ^{125}I by the lactoperoxidase method. The preparation of ^{125}I-labeled PEG-TNF-α was as described elsewhere [12]. PVP-TNF-α was also ^{125}I-labeled in the same way. The biological activities of ^{125}I-labeled native TNF-α, ^{125}I-PEG-TNF-α and ^{125}I-PVP-TNF-α were indistinguishable from those of nonradiolabeled native TNF-α, PEG-TNF-α and PVP-TNF-α, respectively. Meth-A fibrosarcoma cells (4×10^5 cells/mouse) were implanted intradermally into female Balb/c mice. On day 7, when the length of the tumors exceeded 7 mm, the pharmacokinetics of native TNF-α, PEG-TNF-α and PVP-TNF-α were studied. After i.v. injection, blood was collected from the tail vein at indicated times and the radioactivity was measured by a γ-counter. We confirmed that ^{125}I radioactivities in blood were derived from ^{125}I-labeled native TNF-α, ^{125}I-PEG-TNF-α and ^{125}I-PVP-TNF-α by GFC analysis.

3. Results

3.1. Plasma clearance of PEG with various molecular weights

We first compared the plasma clearance of PEGs with various molecular weights (Fig. 1). Elimination profiles of PEGs from the blood circulation varied to a great extent with a change of molecular weight. PEG_{5000} was most rapidly cleared from the circulation; only about 10% of the injected dose remained 20 min after i.v. administration. $PEG_{12,000}$ was retained in the blood circulation for a longer period than PEG_{5000}, but 70% of the injected dose was eliminated after 90 min. In addition, similar elimination profiles were observed for

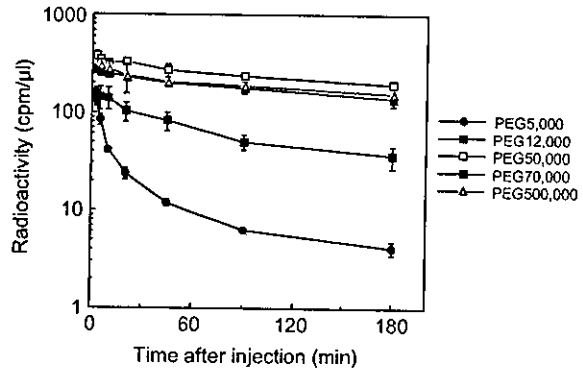

Fig. 1. Plasma clearance of PEGs with various molecular weights in mice bearing S-180 solid tumors after i.v. injection. Mice were intravenously injected with ^{125}I-labeled polymer. After administration, blood was collected from the tail vein at indicated times and the radioactivity was measured by a γ-counter. Mice were used in groups of five. Each value is mean ±SD.

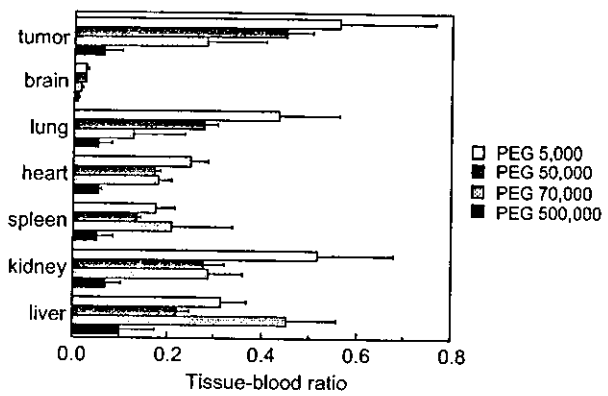

Fig. 2. Tissue distribution of PEGs with various molecular weights in mice bearing S-180 solid tumors after i.v. injection. At 3 h after i.v. injection, mice were sacrificed and each organ was collected. The radioactivity was counted by a γ-counter. Tissue distribution was expressed by the ratio of tissue radioactivity (tissue-cpm/tissue-mg) to blood radioactivity (blood-cpm/blood-mg). Mice were used in groups of five. Each value is mean±SD.

PEGs with molecular weights of more than 50,000. These polymers circulated in blood for a long time.

3.2. Tissue distribution of PEG with various molecular weights

Fig. 2 shows the tissue distribution of PEGs with various molecular weights. The tissue distribution of PEG was suppressed by increasing the molecular weight. In particular, $PEG_{500,000}$ hardly exhibits a tissue distribution. Transport to the brain was extremely restricted for all PEGs. However, a higher polymer distribution in tumors was observed with a molecular weight of less than 50,000. Additionally, $PEG_{70,000}$ tended to be inhibited in terms of the distribution to tumors, and $PEG_{500,000}$ was completely restricted in its transport to tumors in the same as in other tissues. Fig. 3 shows urinary recovery of PEGs with various molecular weights. $PEG_{50,000}$ and $PEG_{500,000}$ were inhibited in terms of urinary excretion, with only 10% of the injected dose being excreted.

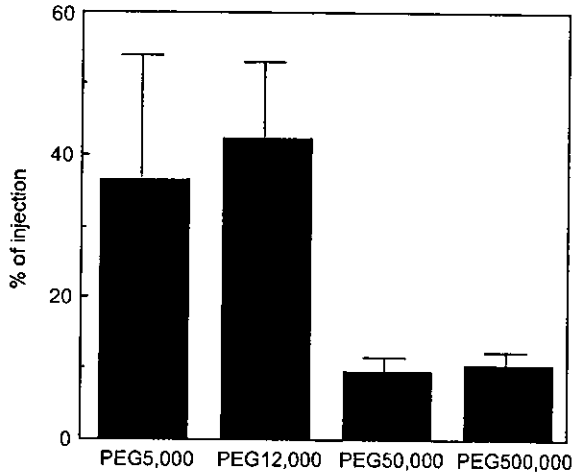

Fig. 3. Urinary excretion of PEGs with various molecular weights in mice bearing S-180 solid tumors after i.v. injection. Mice were housed in metabolic cages to collect urine for 3 h after i.v. injection. The radioactivity of urine was measured by a γ-counter. Mice were used in groups of five. Each value is mean±SD.

3.3. Plasma clearance of various water-soluble polymers

We next studied the elimination profile of various ^{125}I-labeled polymers with the same molecular size after i.v. injection in mice bearing S-180 solid tumors. Pharmacokinetics of ^{125}I-labeled polymers was not influenced by the ^{125}I-labeling method and the preparative method of activated polymers (data not shown). Additionally, almost all radioactivities in blood were derived from ^{125}I-labeled polymers by GFC analysis 3 h after i.v. injection (data not shown). Therefore, it was considered that pharmacokinetics of ^{125}I-labeled polymers was exactly correlative to that of polymers. Fig. 4 illustrates the plasma clearance of various polymers. All polymers showed biphasic elimination patterns. PEG_{5000} and dextran, which are used frequently as drug carriers, were eliminated rapidly from the blood circulation. PDAAm, which has many methyl groups on the side chain of polymer, showed plasma clearance similar to that of PAAm. On the other hand, PVA and PVP circulated longer than the other polymers, while these nonionic polymers had the same molecular size as that of PEG_{5000}. PVP exhibited the longest residence of all the polymers in this study, and 25% of the injected dose remained after 180 min.

Table 1 summarizes the pharmacokinetic parameters of various water-soluble polymers with the same molecular size. Pharmacokinetic analysis revealed

definite differences among each polymer with respect to plasma clearance and tissue distribution. PVP showed the longest MRT of all polymers examined. The total clearance of PVP was about nine-fold lower than that of PEG_{5000}. The distribution volume of dextran was the highest of all these polymers; its volume was 3.4-fold that of PVP. PDAAm showed a higher distribution volume than PAAm. PEG also exhibited a higher distribution volume.

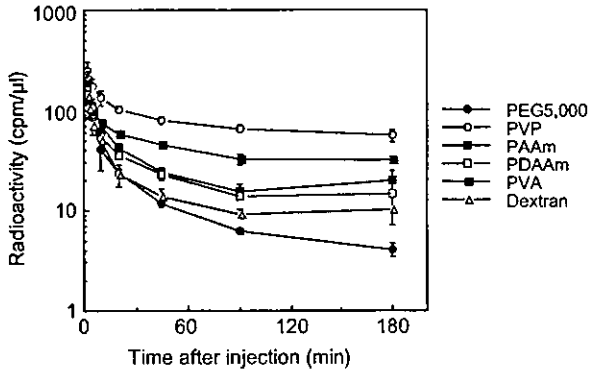

Fig. 4. Plasma clearance of various water-soluble polymers in mice bearing S-180 solid tumors after i.v. injection. Mice were intravenously injected with ^{125}I-labeled polymer. After administration, blood was collected from the tail vein at indicated times and the radioactivity was measured by a γ-counter. Mice were used in groups of five. Each value is mean±SD.

3.4. Tissue distribution of various water-soluble polymers

We next studied the tissue distribution of polymers 3 h after i.v. injection. Although all polymers with the same molecular weight dispersity in this study were nonionic and water-soluble, each polymer showed a characteristic distribution (Fig. 5). Dextran was accumulated in the liver and spleen 3 h after i.v. injection. However, PEG and PVP did not exhibit specific tissue accumulation. PVA, PAAm, and PDAAm showed an increased tendency for tissue distribution than PVP. PVA and PAAm also had no specific distribution, but PDAAm tended to accumulate in the kidney. Fig. 6 shows the urinary excretion of polymers 3 h after i.v. injection.

Table 1
Pharmacokinetic parameters of various water-soluble polymeric modifiers

	Vd_2 (μl))	k_e (min^{-1})	CL_{tot} (μl/min)	MRT (min)
$PEG_{5,000}$	18454.2±2570.3	0.068±0.004	337.2±9.8	78.9±12.4
$PEG_{12,000}$	5128.2±1539.3*	0.017±0.005*	51.7±6.2*	139.5±28.2
PVP	5920.1±193.4	0.013±0.003*	36.7±5.4*	278.8±58.3
PAAm	16833.1±3821.7	0.032±0.008	119.2±25.3*	166.3±73.6
PDAAm	13873.0±1208.5	0.055±0.002	213.1±8.9*	79.7±6.4
PVA	10199.2±991.4	0.010±0.002*	59.3±8.9*	262.5±66.4
Dextran	20034.7±3841.1	0.064±0.008	263.8±23.7	97.6±24.4

The pharmacokinetic parameters of each polymer were evaluated by curve fitting by means of the nonlinear least squares program (MULTI).
Mice were used in groups of five. Each value is the mean±S.E.
Statistical comparisons were made using the Scheffe's method after analysis of variances (ANOVA).
*$P < 0.01$, compared to $PEG_{5,000}$.

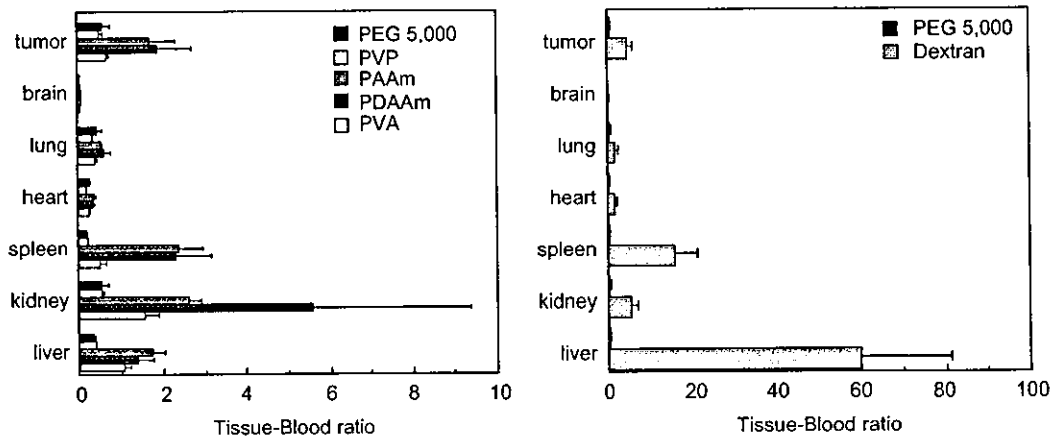

Fig. 5. Tissue distribution of various water-soluble polymers in mice bearing S-180 solid tumors after i.v. injection. At 3 h after i.v. injection, mice were sacrificed and each organ was collected. The radioactivity was counted by a γ-counter. Tissue distribution was expressed by the ratio of tissue radioactivity (tissue-cpm/tissue-mg) to blood radioactivity (blood-cpm/blood-mg). Mice were used in groups of five. Each value is mean±SD.

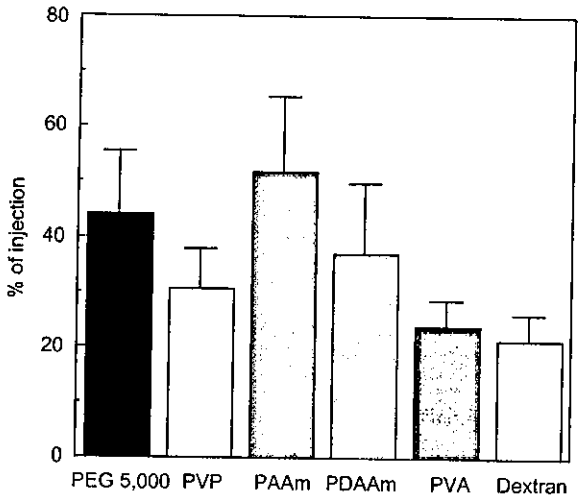

Fig. 6. Urinary excretion of various water-soluble polymers in mice bearing S-180 solid tumors after i.v. injection. Mice were housed in metabolic cages to collect urine for 3 h after i.v. injection. The radioactivity of urine was measured by a γ-counter. Mice were used in groups of five. Each value is mean ± SD.

Table 2
Pharmacokinetic parameters of bioconjugated TNF-α

	$t_{1/2}$ (min)	AUC (0–3 h) (cpm h/μl)	CL_{tot} (μl/min)	k_e ($\times 10^{-3}$/min)
Native TNF-α	4.6±2.2	224±44	47.2±9.6	24.1±8.8
PVP-TNF-α	360.1±45.7	1149±54	4.3±0.5	2.0±0.2
PEG-TNF-α	122.6±85.0	1080±85	3.9±0.3	2.4±0.2

The pharmacokinetic parameters of native and each bioconjugated TNF-α were evaluated by curve fitting by means of non-linear least squares program (MULTI).
Each value is the mean ± S.E.

Urinary recoveries of all polymers were about 20–50% of injected dose. Significant difference was not observed in all polymers examined.

3.5. Plasma clearance of PEG-TNF-α and PVP-TNF-α

We compared the elimination profiles of native TNF-α, PEG-TNF-α and PVP-TNF-α after i.v. injection (Table 2). Native TNF-α was rapidly cleared from the blood. However, PEG-TNF-α and PVP-TNF-α were retained in the blood for an extremely longer period than native TNF-α. In particular, PVP-TNF-α showed a slightly longer circulation lifetime than PEG-TNF-α in spite of the same molecular size.

4. Discussion

This study was aimed at clarifying the pharmacokinetic characteristics of various water-soluble polymers in order to design a bioconjugated drug and to optimize drug delivery based on bioconjugation. Additionally, we estimated the biopharmaceutical disposition of polymers in mice bearing solid tumors in consideration of cancer therapy. ^{125}I-labeled polymers showed the pharmacokinetics in mice bearing solid tumors to be the same as in normal mice (data not shown). This fundamental approach enables us to construct a rational strategy for bioconjugation not only of cytokines but also of various drugs, such as peptides and antineoplasmic agents.

PEG is a low toxic and low antigenic polymeric modifier that has been used for bioconjugation frequently. We have reported that chemical modification of TNF-α with PEG_{5000} markedly and selectively enhanced its antitumor potency when compared to native TNF-α [12]. Additionally, we assessed the relationship among the molecular weight of PEG attached to TNF-α and the degree of modification of PEG-modified TNF-α, their in vivo antitumor potency [13]. As a result, we found that PEG_{5000} is the most suitable polymeric modifier to TNF-α. This phenomenon has also been observed in PEG-modified interleukin-6 [14]. PEG, which was previously considered to be a polymeric modifier suitable for prolonging the circulation lifetime of drugs, was eliminated rapidly from the circulation (Fig. 4, Table 1). This would be mainly because urinary excretion and peripheral distribution volume (Vd_2) of PEG were relatively high (Table 1). PEG is a polyether diol of general structure $HO\text{-}(CH_2CH_2O)_n\text{-}H$, where functionalization of PEG is restricted only to the utilization of terminal primary OH groups [15]. From this viewpoint, modifiable polymeric modifiers are needed to control the biopharmaceutical characteristics of conjugated drugs. Therefore, we assessed the pharmacokinetic profile of various water-soluble polymers with molecular size of about 5000, and compared their pharmacokinetics to PEG_{5000}.

Dextran was accumulated in the liver and spleen (Fig. 5). As demonstrated clearly in Fig. 4, dextran is not appropriate for prolonging the circulation time of drugs. Polysaccharides are captured by the cells of the reticloendothelial system (RES), mainly by the liver. Therefore, it is considered that dextran is rapidly eliminated from the circulation. PVP, which can be linked with various comonomers in order to control the physicochemical properties, had the longest circulation lifetime (Fig. 4). In addition, its tissue distribution was extremely restricted (Fig. 5). The fate and distribution of conjugates between polymeric carriers and drugs can be influenced by the properties of the polymer. For example, recently, we showed polyvinylpyrrolidone-co-dimethyl maleic anhydride [poly(VP-co-DMMAn)] accumulated in the kidney (about 80% of administered dose) 24 h after intravenous injection. Additionally, conjugates between poly(VP-co-DMMAn) and

anti-inflammatoric proteins also accumulated in the kidney and accelerated recovery from acute renal failure. PVP had the longest circulation time and, its tissue distribution was extremely restricted. In addition, it is easy to introduce various comonomers on radical polymerization to PVP. These results suggest that PVP is the most feasible polymeric modifier for localizing the conjugated drug in blood. In fact, PVP-TNF-α showed a longer plasma half-life than PEG-TNF-α, and the plasma half-life of PVP-TNF-α was 90-fold higher than that of native TNF-α. As a result, PVP-TNF-α had a more potent antitumor effect than PEG-TNF-α (data not shown). Modification with polymeric modifiers such as PEG has also been used to stabilize the liposome in vivo [16] and to control the pharmacokinetics of nanoparticle carriers [17]. Therefore, PVP can be adopted not only to the bioconjugation of drugs but also to the steric stabilization of liposomes in vivo and the surface modification of particle carriers. The pharmacokinetic properties of polymers was influenced by various reasons: (1) the interaction of endothelial cells in tissues; (2) the ratio of glomerular filtration (it was influenced by the properties of polymer, such as electric charge, hydrophilic–lipophilic balance, the ability of binding to plasma proteins, and shape of polymer in blood). In dextran, we showed that dextran did not interact with bovine aortic endothelial cell (BAEC) (unpublished data). However, other researchers showed that dextran was adsorbed in rat liver parenchymal and nonparenchymal cells. Therefore, dextran may accumulate in the liver. In PEG, PVA and PAAm, we showed that these polymers did not interact with BAEC. Therefore, we considered that these polymers had long circulation time. Whereas the difference of structure was only addition of dimethyl groups, PDAAm tended to distribute in the kidney compared with PAAm. I did not have any data to explain this difference. To clarify this mechanism, we now examine the ability of PAAm to bind to endothelial cells in the kidney and renal proximal epithelial cells. PVP had the longest circulation time among polymers, and its tissue distribution was extremely restricted. It was suggested that the ability of polymer to bind to plasma protein influenced the pharmacokinetic of polymer. For example, the poly(styrene-co-maleic anhydride) (SMA) has been shown to bind to plasma albumin. SMA-conjugated neocarzinostatin (SMANCS) binds rapidly to plasma albumin when injected intravenously and showed much longer plasma half-lives. Therefore, we examined the ability of PVP to bind albumin. However, PVP did not bind to albumin. Now, we are examining the ability of PVP to bind to other plasma protein. Another idea that can explain the longer half-life of PVP is the difference of shape in blood due to the local motion of polymer. We are now examining the polymer chain dynamics in blood by computational simulation and experiment, such as the fluorescence depolarization method. On the other hand, it is well known that the permeability is very high in tumor tissue. Therefore, we studied the pharmacokinetics of polymers with various molecular sizes on the model of PEG. PEGs showed different circulation lifetimes, tissue distribution, and urinary excretion with a change of molecular weight (Figs. 1–3). These results indicate that optimum drug delivery might be achieved by considering the permeability of each organ (size barrier).

The modification of proteins and peptides by covalent attachment of polymeric modifiers can eliminate some drawbacks of native proteins and peptides and improve their physicochemical, biomedical, and pharmacological characteristics. These benefits of bioconjugation lead to the production of many chemically modified drugs, such as PEG-ADA and SMANCS, and dramatic therapeutic effects have been reported [18,19]. These approaches also exhibited that the fate and distribution of the conjugates were attributed to the physicochemical properties of polymeric modifiers. In addition, various polymeric modifiers for bioconjugation have been developed. However, with the exception of a few examples, drug therapy based on bioconjugation has not been applied for clinical use. The reason for this is that the methodology of bioconjugation has not been established for many drug therapies using antineoplasmic agents or cytokines, which needs strict control relative to targeting site and therapeutic concentration pattern. In addition, a methodology, for example, based on optimum selection of polymeric modifiers for specific characteristics of drugs and for the purpose of bioconjugation, as well as a mode of attachment, has not yet been established. Our fundamental approach will enable us to establish such a methodology of bioconjugation.

However, our approach to the molecular design of polymeric modifiers has involved only a few steps. Our previous study showed that nonionic polymers did not interact with endothelial cells, but the increase of interaction between polymers and endothelial cells is parallel to the amount of charge or hydrophobic groups (unpublished data). Therefore, we must investigate the relation between several biological factors, such as endothelial cells or plasma proteins and the physicochemical disposition, which is typified by the charge or the hydrophilic–hydrophobic balance in order to resolve the biopharmaceutical characteristics of polymeric modifiers. This approach may facilitate the optimum molecular design of polymeric modifiers in a drug delivery system.

5. Conclusion

PVP had the longest circulation lifetime among various polymers and its tissue distribution was extremely

restricted. PVP-TNF-α showed longer plasma half-life than PEG-TNF-α, and the plasma half-life of PVP-TNF-α was 90-fold higher than that of native TNF-α. These results suggest that PVP is the most suitable polymeric modifier for prolonging the circulation lifetime of a drug and localizing the conjugated drug in blood.

Acknowledgements

This study was supported in part by a Grant-in-Aid for Scientific Research (No. 15680014) from the Ministry of Education, Science and Culture of Japan, and in part by Health Sciences Research Grants for Research on Health Sciences focusing on Drug Innovation from the Japan Health Sciences Foundation (KH63124), and in part by Takeda Science Foundation.

References

[1] Furman WL, Strother D, McClain K, Bell B, Leventhal B, Pratt CB. Phase I clinical trial of recombinant human tumor necrosis factor in children with refractory solid tumors: a pediatric oncology group study. J Clin Oncol 1993;11:2205–10.

[2] Kreitman RJ, Wilson WH, Bergeron K, Raggio M, Stetler-Stevenson M, FitzGerald DJ, Pastan I. Efficacy of the anti-CD22 recombinant immunotoxin BL22 in chemotherapy-resistant hairy-cell leukemia. N Engl J Med 2001;345:241–7.

[3] Glue P, Rouzier-Panis R, Raffanel C, Sabo R, Gupta SK, Salfi M, Jacobs S, Clement RP. A dose-ranging study of pegylated interferon alfa-2b and ribavirin in chronic hepatitis C. The Hepatitis C Intervention Therapy Group. Hepatology 2000;32:647–53.

[4] Barnard DL. Pegasys (Hoffmann-La Roche). Curr Opin Invest Drug 2001;2:1530–8.

[5] Tsutsumi Y, Onda M, Nagata S, Lee B, Kreitman RJ, Pastan I. Site-specific chemical modification with polyethylene glycol of recombinant immunotoxin anti-Tac(Fv)-PE38 (LMB-2) improves antitumor activity and reduces animal toxicity and immunogenicity. Proc Natl Acad Sci USA 2000;97:8548–53.

[6] Kamada H, Tsutsumi Y, Yamamoto Y, Kihira T, Kaneda Y, Mu Y, Kodaira H, Tsunoda SI, Nakagawa S, Mayumi T. Antitumor activity of tumor necrosis factor-alpha conjugated with polyvinylpyrrolidone on solid tumors in mice. Cancer Res 2000;60:6416–20.

[7] Kaneda Y, Yamamoto Y, Kamada H, Tsunoda S, Tsutsumi Y, Hirano T, Mayumi T. Antitumor activity of tumor necrosis factor alpha conjugated with divinyl ether and maleic anhydride copolymer on solid tumors in mice. Cancer Res 1998;58:290–5.

[8] Kamada H, Tsutsumi Y, Sato-Kamada K, Yamamoto Y, Yoshioka Y, Okamoto T, Nakagawa S, Nagata S, Mayumi T. Synthesis of a poly(vinylpyrrolidone-co-dimethyl maleic anhydride) co-polymer and its application as renal targeting carrier. Nat Biotechnol 2003;21:399–404.

[9] Yamamoto Y, Tsutsumi Y, Yoshioka Y, Nishibata T, Kobayashi K, Okamoto T, Mukai Y, Shimizu T, Nakagawa S, Nagata S, Mayumi T. Site-specific PEGylation of a lysine-deficient TNF-alpha with full bioactivity. Nat Biotechnol 2003;21:546–52.

[10] Inoue M, Ebashi I, Watanabe N, Morino Y. Synthesis of a superoxide dismutase derivative that circulates bound to albumin and accumulates in tissues whose pH is decreased. Biochemistry 1989;28:6619–24.

[11] Yamaoka K, Tanigawara Y, Nakagawa T, Uno T. A pharmacokinetic analysis program (multi) for microcomputer. J Pharmacobiodyn 1981;4:879–85.

[12] Tsutsumi Y, Kihira T, Tsunoda S, Kanamori T, Nakagawa S, Mayumi T. Molecular design of hybrid tumour necrosis factor alpha with polyethylene glycol increases its anti-tumour potency. Br J Cancer 1995;71:963–8.

[13] Tsutsumi Y, Tsunoda S, Kamada H, Kihira T, Nakagawa S, Kaneda Y, Kanamori T, Mayumi T. Molecular design of hybrid tumour necrosis factor-alpha. II: The molecular size of polyethylene glycol-modified tumour necrosis factor-alpha affects its anti-tumour potency. Br J Cancer 1996;74:1090–5.

[14] Tsutsumi Y, Tsunoda S, Kamada H, Kihira T, Kaneda Y, Ohsugi Y, Mayumi T. PEGylation of interleukin-6 effectively increases its thrombopoietic potency. Thromb Haemost 1997;77:168–73.

[15] Nagasaki Y, Iijima M, Kato M, Kataoka K. Primary amino-terminal heterobifunctional poly(ethylene oxide). Facile synthesis of poly(ethylene oxide) with a primary amino group at one end and a hydroxyl group at the other end. Bioconjug Chem 1995;6:702–4.

[16] Torchilin VP, Trubetskoy VS, Whiteman KR, Caliceti P, Ferruti P, Veronese FM. New synthetic amphiphilic polymers for steric protection of liposomes in vivo. J Pharm Sci 1995;84:1049–53.

[17] Peracchia MT, Vauthier C, Puisieux F, Couvreur P. Development of sterically stabilized poly(isobutyl 2-cyanoacrylate) nanoparticles by chemical coupling of poly(ethylene glycol). J Biomed Mater Res 1997;34:317–26.

[18] Hershfield MS. PEG-ADA replacement therapy for adenosine deaminase deficiency: an update after 8.5 years. Clin Immunol Immunopathol 1995;76:S228.

[19] Konno T. Targeting chemotherapy for hepatoma: arterial administration of anticancer drugs dissolved in Lipiodol. Eur J Cancer 1992;28:403–9.

FEBS Letters 560 (2004) 178–182 FEBS 28108

RNA interfering approach for clarifying the PPARγ pathway using lentiviral vector expressing short hairpin RNA

Kazufumi Katayama[a], Koichiro Wada[b,*], Hiroyuki Miyoshi[c], Kozo Ohashi[a], Masashi Tachibana[a], Rie Furuki[a], Hiroyuki Mizuguchi[d], Takao Hayakawa[d], Atsushi Nakajima[e], Takashi Kadowaki[f], Yasuo Tsutsumi[a], Shinsaku Nakagawa[a], Yoshinori Kamisaki[b], Tadanori Mayumi[a]

[a] *Department of Biopharmaceutics, Graduate School of Pharmaceutical Science, Osaka University, Osaka 565-0871, Japan*
[b] *Department of Pharmacology, Graduate School of Dentistry, Osaka University, 1-8 Yamadaoka, Suita, Osaka 565-0871, Japan*
[c] *Subteam for Manipulation of Cell Fate, BioResource Center, RIKEN, Tsukuba Institute, Ibaraki, Japan*
[d] *Division of Biological Chemistry and Biologicals, National Institute of Health Sciences, Tokyo 158-8501, Japan*
[e] *The Third Department of Internal Medicine, Yokohama City University School of Medicine, Yokohama 236-0004, Japan*
[f] *Department of Metabolic Diseases, Graduate School of Medicine, University of Tokyo, Tokyo, 113-0033, Japan*

Received 15 December 2003; revised 10 January 2004; accepted 22 January 2004

First published online 4 February 2004

Edited by Robert Barouki

Abstract Peroxisome proliferator-activated receptor γ(PPARγ) plays a central role in adipocyte differentiation and insulin sensitivity. Although PPARγ also appears to regulate diverse cellular processes in other cell types such as lymphocytes, the detailed mechanisms remain unclear. In this study, we established a lentivirus-mediated short hairpin RNA expression system and identified a potent short hairpin RNA which suppresses PPARγ expression, resulting in marked inhibition of preadipocyte-to-adipocyte differentiation in 3T3-L1 cells. Our PPARγ-knockdown method will serve to clarify the PPARγ pathway in various cell types in vivo and in vitro, and will facilitate the development of therapeutic applications for a variety of diseases.

Key words: Peroxisome proliferator-activated receptor γ; RNA interference; Short hairpin RNA; Lentiviral vector; Adipocyte

1. Introduction

The peroxisome proliferator-activated receptor (PPAR) family was discovered as an orphan nuclear receptor, and three different subtypes were subsequently identified, namely PPARα, PPARδ/β and PPARγ. PPARγ is abundantly expressed in adipose tissue and plays a key role in adipocyte differentiation and insulin sensitivity [1]. Recently, our group and other researchers reported that PPARγ is also an attractive therapeutic target as it can play an important role in immune responses, especially in transcriptional regulation of inflammatory responses [2–5].

The biological role of PPARγ had been widely investigated by using PPARγ-deficient mice generated by targeted disruption of the PPARγ gene. Since homozygous PPARγ-deficient mice ($PPAR\gamma^{-/-}$) are embryonic lethal due to placental dysfunction [1], heterozygous mice ($PPAR\gamma^{+/-}$) have been used to investigate the role of PPARγ in vivo experiments. However, $PPAR\gamma^{+/-}$ mice seem to be of limited use in some experiments, because PPARγ also appears to regulate diverse cellular processes in cells that show lower levels of PPARγ expression in comparison to adipose tissue [6,7].

RNA interference (RNAi) is a powerful technique for selectively silencing the expression of genes. Recent work has provided a system for the stable expression of short interfering RNA (siRNA) in mammalian cells, which is generally based on the expression of short hairpin RNA (shRNA) under the control of the RNA polymerase III promoter [8–11]. The technique has allowed for the development of a new approach for achieving targeted gene silencing of disease-associated genes in animal models as well as in cultured cells.

Lentiviral vectors (LVs) are a promising tool for exogenous gene transfer among gene transfer vehicles, because LVs have the advantages of infecting non-dividing cells and being stably integrated into the host genome resulting in long-term expression of transgene [12–16]. Furthermore, recent reports have demonstrated that virus-mediated RNAi could provide long-term silencing in mammalian cells [9,17,18]. In the present study, we attempted to develop a technique for suppressing the expression of PPARγ in vivo and in vitro. We established a lentivirus-mediated shRNA expression system and identified a potent shRNA target sequence in the coding region of PPARγ mRNA. This approach has enabled us to clarify a novel role of PPARγ.

2. Materials and methods

2.1. Vector construction

Vectors were constructed using standard cloning procedures. H1-RNA promoter was amplified from human genomic DNA (Clontech, Palo Alto, CA, USA) using the following primers: 5′-CCATGGAATTCGAACGCTGACGTC-3′ and 5′-GCAAGCTTAGATCTGTGGTCTCATACAGAACTTATAAGATTCCC-3′. The amplified polymerase chain reaction (PCR) product was inserted into the *Eco*RI-*Bgl*II site of pHM5 [19], generating pHM5-H1. pHM5-H1 was designed to express shRNA upon the insertion of an appropriate sequence into the *Bgl*II/*Xba*I site (Fig. 1A). Oligonucleotides encoding

*Corresponding author. Fax: (81)-6-6879 2914.
E-mail address: kwada@dent.osaka-u.ac.jp (K. Wada).

Abbreviations: LV, lentiviral vector; shRNA, short hairpin RNA; MOI, multiplicity of infection; PPAR, peroxisome proliferator-activated receptor; GPDH, glycerol-3-phosphate dehydrogenase; BRL, rosiglitazone (BRL-49653)

0014-5793/04/$30.00
doi:10.1016/S0014-5793(04)00100-0

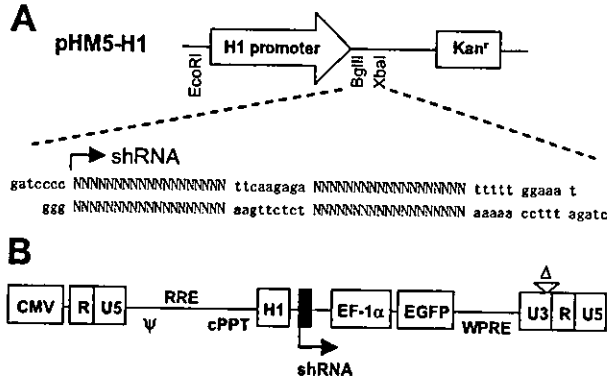

Fig. 1. Vector construction. A: pHM5-H1 was constructed as described in Section 2. Oligonucleotides encoding both strands of the targeting sequence, a spacer sequence which provided a loop structure and a transcriptional termination signal T5 were annealed and inserted into *BglII*/*XbaI* sites in pHM5-H1. B: Schematic representation of self-inactivating (SIN) LV plasmid (CS-H1-shRNA-EG). CMV: cytomegalovirus promoter, Ψ: packaging signal, RRE: rev responsive element, cPPT: central polypurine tract, H1: human H1 promoter, EF-1α: human elongation factor 1α subunit gene promoter, EGFP: enhanced green fluorescent protein, WPRE: woodchuck hepatitis virus posttranscriptional regulatory element. Δ: deleting 133 bp in the U3 region of the 3′ long terminal repeat.

both strands of the targeting sequence were annealed and inserted into *BglII*/*XbaI* sites of pHM5-H1 (Fig. 1A and Table 1). The sequence was verified on a DNA sequencer (ABI Prism 310, Applied Biosystems) and the cassette containing the H1 promoter plus the shRNA was transferred to a self-inactivating (SIN) LV construct, generating CS-H1-shRNA-EG (Fig. 1B).

2.2. Preparation of LV expressing shRNA (LV-shRNA)

LVs pseudotyped with vesicular stomatitis virus G glycoprotein (VSV-G) were prepared according to a previously described method [15,20,21]. Briefly, 293T cells were transfected with four plasmids: packaging construct (pMDLg/pRRE), VSV-G-expressing construct (pMD.G), Rev-expressing construct (pRSV-Rev), and SIN vector construct (CS-H1-shRNA-EG). Vector supernatant was concentrated by ultracentrifugation, and the pellet was resuspended in Hanks' balanced salt solution. Vector titers, which can be detected by enhanced green fluorescent protein (EGFP) expression under the control of a human elongation factor 1α subunit gene promoter, were determined by infection of HeLa P4 cells with serial dilutions of the vector stocks, followed by fluorescence-activated cell sorter (FACS) analysis for EGFP-positive cells.

2.3. Cell culture and infection of LV-shRNA

3T3-L1 preadipocytes were cultured in Dulbecco's modified Eagle's medium supplemented with 10% fetal bovine serum. The 3T3-L1 cells were infected with viral stocks at a multiplicity of infection (MOI) of 50 or 200, followed by FACS analysis for EGFP expression. Transduction efficiencies were 66.57%±1.44 at 50 MOI and 91.64%±1.07 at 200 MOI, expressed as S.E.M. The transduced 3T3-L1 cells were grown and then used in subsequent experiments.

2.4. Differentiation protocol

Induction of adipocyte differentiation was performed essentially as described [22]. Two days after confluence (day 0), the medium was replaced with differentiation medium containing rosiglitazone (BRL, 1 μM), insulin (INS, 150 nM), dexamethasone (DEX, 1 μM) and 3-isobutyl-1-methylxanthine (IBMX, 100 μM), which was changed every 3 days thereafter until analysis.

2.5. Measurement of adipocyte differentiation

Differentiation of 3T3-L1 preadipocytes to adipocytes was monitored by measurement of intracellular lipid accumulation using Oil red O staining and glycerol-3-phosphate dehydrogenase (GPDH) activity on day 9. Cultured cells were fixed for 2 h with 10% formalin in isotonic phosphate buffer and then washed with distilled water. The cells were then stained by complete immersion in a working solution (0.3%) of Oil red O for 4 h. Excess dye was removed by exhaustive washing with water. The GPDH activity was measured using a GPDH assay kit (Hokudo, Hokkaido, Japan).

2.6. RNA isolation and reverse transcription (RT) PCR analysis

Total RNA was extracted from the 3T3-L1 cells infected with each kind of LV-shRNA using Tri-Reagent (Sigma). First-strand cDNA was generated from 1 μg of RNA by using oligo(dT_{12-18}) primer (Invitrogen) and SuperScript III RNase H Reverse Transcriptase (Invitrogen) according to the manufacturer's protocol. The reverse transcription reaction mix was amplified with the following pair of oligonucleotides specific for murine PPARα, PPARδ, PPARγ2 and glyceraldehyde-3-phosphate dehydrogenase (GAPDH): PPARα, 5′-CGACAAGTGTGATCGGAGCTGCAAG-3′ and 5′-GTTGAAGTTCTTCAGGTAGGCTTC-3′; PPARδ, 5′-GGCCAACGGCAGTGGCTTCGTC-3′ and 5′-GGCTGCGGCCTTAGTACATGTCCT-3′; PPARγ2, 5′-GCTGTTATGGGTGAAACTCTG-3′ and 5′-ATAAGGTGGAGATGCAGGTTC-3′; GAPDH, 5′-GCTCACTGGCATGGCCTTC-3′ and 5′-ACCACCCTGTTGCTGTAGC-3′ [23]. The sample was amplified in the linear phase, optimized for each gene (PPARα: 38 cycles; PPARδ: 30 cycles; PPARγ2: 36 cycles; GAPDH: 23 cycles). All PCR products were electrophoresed on 2% agarose gel using 0.5×Tris-borate-EDTA buffer and visualized using ethidium bromide. The gel image was captured by a digital camera, and densitometric analysis was performed using NIH Image software.

2.7. Western blot analysis

Cultured cells were homogenized in Tris–HCl buffer containing a cocktail of protease inhibitors and insoluble materials were then removed by centrifugation at 4°C. The solubilized lysates were resolved by sodium dodecyl sulfate–polyacrylamide gel electrophoresis under reducing conditions at a concentration of 5 μg protein of sample per lane. Detection of PPARα, PPARδ, PPARγ and GAPDH was respectively performed with anti-PPARα polyclonal antibody (Santa Cruz Biotechnology, Santa Cruz, CA, USA), anti-PPARδ polyclonal antibody (Santa Cruz Biotechnology), anti-PPARγ monoclonal antibody (Santa Cruz Biotechnology) and anti-GAPDH polyclonal antibody (Trevigen, Gaithersburg, MD, USA) according to a previously described method [4]. The band intensity was quantified using NIH Image software.

2.8. Statistical analysis

All results are expressed as mean±S.E.M. Statistical comparisons were made with Student's *t*-test or Scheffé's method after analysis of variances. The results were considered significantly different at $P<0.05$.

Table 1
LV vectors used in this study

LV vector	shRNA target gene	shRNA target sequence
LV-shRNA-P11	PPARγ1 and 2	CAGCTCTACAACAGGCCTC
LV-shRNA-P12	PPARγ1 and 2	ATGGCCATTGAGTGCCGAG
LV-shRNA-P13	PPARγ1 and 2	TAAATGTCAGTACTGTCGG
LV-shRNA-P14	PPARγ1 and 2	TTGGCGGAGATCTCCAGTG
LV-shRNA-P15	PPARγ1 and 2	GTCTGCTGATCTGCGAGCC
LV-shRNA-P16	PPARγ1 and 2	TCACCATTTGTCATCTACG
LV-shRNA-P17	PPARγ1 and 2	GTTTGAGTTTGCTGTGAAG
LV-shRNA-P18	PPARγ1 and 2	ATGAGCCTTCACCCCCTGC
LV-shRNA-P19	PPARγ1 and 2	GATCTGCGAGCCCTGGCAA
LV-shRNA-P21	PPARγ2	ACTCTGGGAGATTCTCCTG
LV-shRNA-P22	PPARγ2	CCTTCGCTGATGCACTGCC
LV-shRNA-Lu	Luciferase	ACGCTGAGTACTTCGAAAT
LV-shRNA-Scramble	No target gene	GCGCGCTTTGTAGGATTCG
LV-EG	–	–

LV-EG has no shRNA-expressing cassette. All vectors carry an EGFP-expressing cassette as a marker gene so that the cells transduced with LV-shRNAs can be identified by green fluorescence.

3. Results and discussion

To develop an effective PPARγ-knockdown method, we constructed an LV-based siRNA system in which shRNA encoding both strands of the targeting sequence is expressed under the control of human H1 promoter [24]. A human H1 promoter was cloned to generate pHM5-H1, and oligonucleotide encoding shRNA against PPARγ mRNA was inserted (Fig. 1A). Subsequently, the cassette containing the H1 promoter plus the shRNA was transferred to the SIN LV construct (Fig. 1B). Using a shRNA target sequence against firefly luciferase, we previously demonstrated that our LV-based siRNA system effectively suppressed the target gene in mammalian cells (data not shown).

PPARγ exists as two isoforms, termed PPARγ1 and PPARγ2,

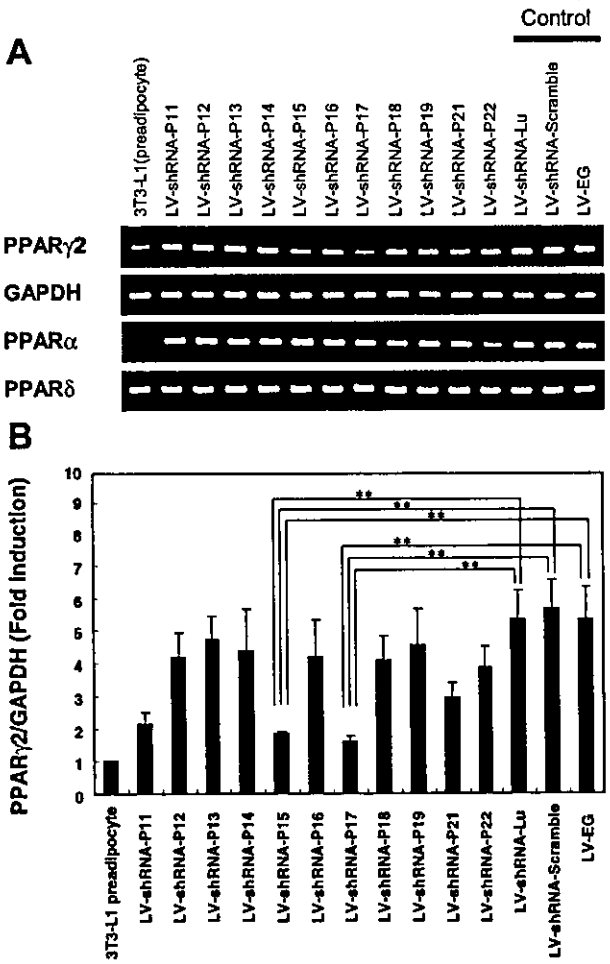

Fig. 2. Alteration of PPAR family mRNA levels in 3T3-L1 cells transduced with LV-shRNAs. A: 3T3-L1 preadipocytes were infected with each LV-shRNA (200 MOI) and then subjected to the differentiation protocol. Two days after the induction of adipocyte differentiation, mRNA levels of PPARγ2, PPARα, PPARδ, and GAPDH were determined by RT-PCR analysis. Results are representative gel images. B: Densitometric quantitation for PPARγ and GAPDH from three to four independent experiments. Each PPARγ value was normalized to the values for GAPDH and expressed as fold induction over the basal level detected in 3T3-L1 preadipocytes (bars, S.E.M.). $^{**}P < 0.01$ for LV-shRNA-P15 and -P17 compared with LV-shRNA-Lu, LV-shRNA-Scramble or LV-EG.

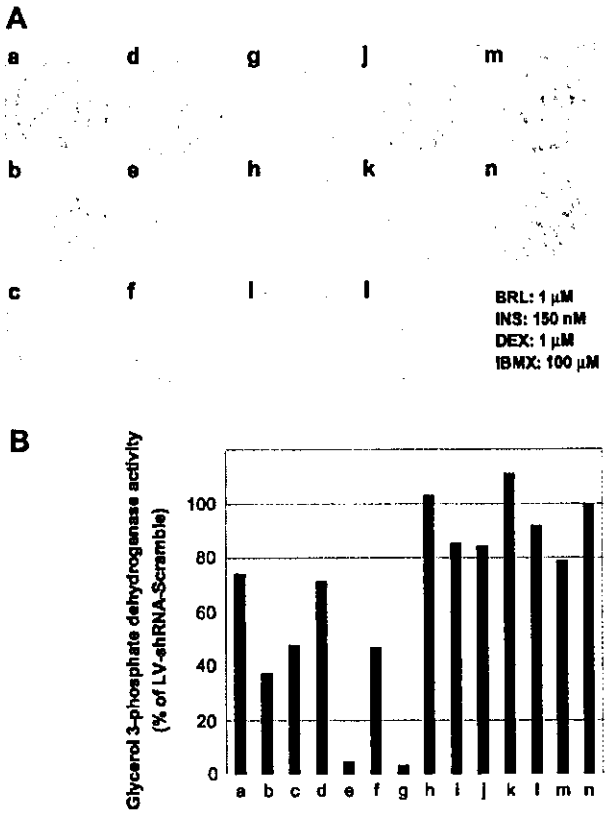

Fig. 3. Effect of LV-shRNAs on adipocyte differentiation. A: Differentiation of 3T3-L1 preadipocytes (infected with LV-shRNA; 200 MOI) to adipocytes was monitored by measurement of intracellular lipid accumulation using Oil red O staining on day 9. B: GPDH activity was measured on day 9. Data were expressed as percentage of the GPDH activity of 3T3-L1 cells which were infected with LV-shRNA-Scramble (200 MOI). a: LV-shRNA-P11; b: LV-shRNA-P12; c: LV-shRNA-P13; d: LV-shRNA-P14; e: LV-shRNA-P15; f: LV-shRNA-P16; g: LV-shRNA-P17; h: LV-shRNA-P18; i: LV-shRNA-P19; j: LV-shRNA-P21; k: LV-shRNA-P22; l: LV-EG; m: LV-shRNA-Lu; n: LV-shRNA-Scramble. Similar results were obtained in two independent experiments.

which are produced by a combination of different promoters and alternative splicing. PPARγ2 has an N-terminal extension of 30 amino acids and is very highly expressed in adipocytes [22,25]. We selected 11 target sequences in the coding region of PPARγ mRNA and constructed LV-shRNAs against PPARγ (Table 1). In the present study, LV-shRNA-Lu, LV-shRNA-Scramble and LV-EG were used as controls.

To find the most effective shRNA target sequence against PPARγ, we analyzed the silencing of PPARγ in 3T3-L1 cells during preadipocyte-to-adipocyte differentiation in which PPARγ is known to be a master regulator of adipogenesis [1,26,27]. The expression of PPARγ increases during the differentiation process and activation of PPARγ protein by its ligand leads to adipogenesis through the activation of the adipogenic gene cascade. The 3T3-L1 preadipocytes transduced with each of the LV-shRNAs, i.e. 3T3-L1 cells expressing shRNAs, as listed in Table 1, were exposed to differentiation medium (DM) 2 days after confluence (day 0). Initially, silencing of PPARγ expression was examined by RT-PCR after 2 days of culture in DM (Fig. 2). Although 3T3-L1 cells transduced with LV-shRNA-Lu, -Scramble and LV-EG showed

significant increases in the levels of PPARγ mRNA, 3T3-L1 cells transduced with LV-shRNA-P15 and -P17 retained low levels of PPARγ mRNA comparable to the level in preadipocytes maintained in normal culture medium. In contrast, the expression levels of GAPDH, PPARα and PPARδ were not altered by LV-shRNA-P15 or -P17. The other LV-shRNAs against PPARγ caused moderate decreases in the levels of PPARγ mRNA.

The differentiation of 3T3-L1 preadipocytes to adipocytes can be monitored by measurement of intracellular lipid accumulation and GPDH (an important enzyme in triglyceride synthesis) activity [28–30]. Intracellular lipid accumulation was dramatically reduced in the LV-shRNA-P15- and -P17-infected 3T3-L1 cells as shown by Oil red O staining (Fig. 3A, e: LV-shRNA-P15; g: LV-shRNA-P17). GPDH activity also demonstrated that LV-shRNA-P15 and LV-shRNA-P17 express a potent shRNA which suppresses PPARγ mRNA expression, resulting in marked inhibition of preadipocyte-to-adipocyte differentiation (Fig. 3B). We also confirmed that the expression of PPARγ-inducible genes, such as uncoupling protein-1 and adipocyte fatty acid binding protein, were inhibited in 3T3-L1 cells transduced with LV-shRNA-P15 and LV-shRNA-P17 in the presence of the PPARγ-specific ligand, BRL (unpublished data).

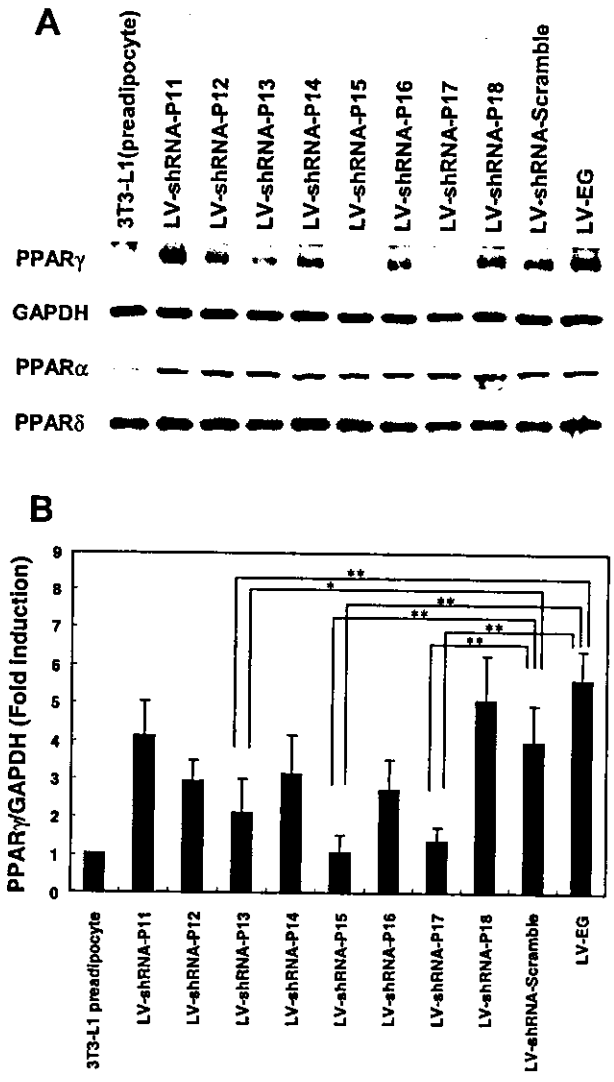

Fig. 4. Alteration of PPAR family protein levels in 3T3-L1 cells transduced with LV-shRNAs (200 MOI). A: Four days after the induction of adipocyte differentiation, the whole cell extract was analyzed by Western blotting with antibodies against PPARγ, PPARα, PPARδ and GAPDH. Results are representative of three individual experiments. B: Densitometric quantitation for PPARγ and GAPDH from three individual experiments. Each PPARγ value was normalized to the values for GAPDH and expressed as fold induction over the basal level detected in 3T3-L1 preadipocytes (bars, S.E.M.). $^{**}P<0.01$ for LV-shRNA-P13, -P15 and -P17 compared with LV-shRNA-Scramble or LV-EG. $^{*}P<0.05$ for LV-shRNA-P13 compared with LV-EG.

A recent study demonstrated that if the degree of complementarity to its target is reduced, siRNA can function as microRNAs which affect translational suppression without cleavage [31]. An important objective of this study was to determine whether the silencing effect of PPARγ caused by these LV-shRNAs was specific for PPARγ. In fact, several shRNA target sequences used in this study partially correspond to PPARα or PPARδ. Western blotting analysis demonstrated that PPARγ protein levels were significantly decreased in the LV-shRNA-P15- and LV-shRNA-P17-infected 3T3-L1 cells, while LV-shRNAs did not alter the amount of PPARα, PPARδ or GAPDH protein (Fig. 4). These results were consistent with the result from RT-PCR analysis (Fig. 2).

Furthermore, we examined 3T3-L1 cells exposed to either LV-shRNA-Scramble, -P15 or -P17 by fluorescent microscopy for EGFP expression to identify cells not infected with those vectors, i.e. the 3T3-L1 cells not expressing the shRNA encoded by LV-shRNA-P15 or -P17 (Fig. 5). In the case of LV-shRNA-Scramble, which expresses control shRNA, the differentiation of preadipocytes to adipocytes was not affected by infection with LV. In contrast, all of the cells infected with LV-shRNA-P15 or -P17 retained their fibroblast-like morphology. Taken together, these results indicate that our LV-shRNA-based PPARγ-knockdown method resulted in decreased PPARγ expression and specific inhibition of the PPARγ pathway, even in the case of adipocyte differentiation in which PPARγ expression is strongly induced by DM and PPARγ protein is effectively activated by the PPARγ-specific ligand used in this study, BRL.

Accessibility of the siRNA might depend on the secondary structure of the target mRNA. However, a clear correlation between either secondary structure or GC content and effectiveness of target sites has not yet been recognized. Although we designed 11 different shRNAs against PPARγ, we have not found any correlation between several factors that have been implicated in the accessibility of transcriptional/translational regulatory elements and effectiveness of target sites of shRNA until now.

In the present study, we developed a promising tool for suppressing the expression of PPARγ. Our PPARγ-knockdown method will serve to clarify the role of the PPARγ pathway in various cell types in vivo and in vitro, and will facilitate the development of therapeutic applications for a variety of diseases.

Acknowledgements: This work was supported in part by a grant (Tokuteiryouiki C13204072, to A.N.) from the Ministry of Education, Culture, Sports, Science and Technology, and a grant (15590227, to K.W.) from the Japan Society for the Promotion of Science.

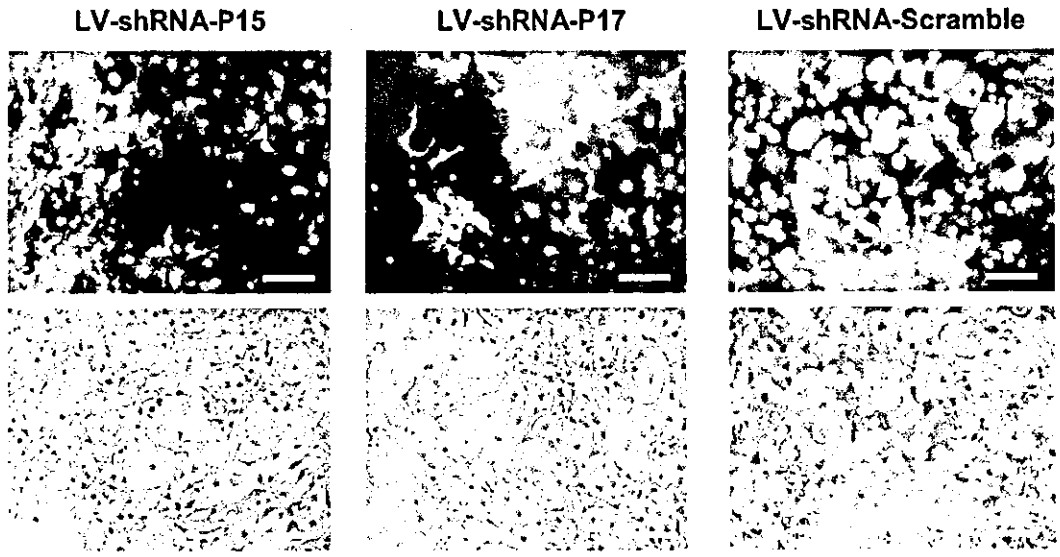

Fig. 5. Identification of the 3T3-L1 cells transduced with LV-shRNA. Brightfield and fluorescent microscopy images collected from the same field. The LV-shRNA-infected cells, which expressed EGFP, were detected as green fluorescence (upper panels) and morphologically identified mature adipocyte with a voluminous spherical shape and a large accumulation of intracytoplasmic lipid vesicles (lower panels). Bars represent 100 μm.

References

[1] Kubota, N. et al. (1999) Mol. Cell 4, 597–609.
[2] Su, C.G. et al. (1999) J. Clin. Invest. 104, 383–389.
[3] Desreumaux, P. et al. (2001) J. Exp. Med. 193, 827–838.
[4] Nakajima, A. et al. (2001) Gastroenterology 120, 460–469.
[5] Katayama, K. et al. (2003) Gastroenterology 124, 1315–1324.
[6] Schlezinger, J.J., Jensen, B.A., Mann, K.K., Ryu, H.Y. and Sherr, D.H. (2002) J. Immunol. 169, 6831–6841.
[7] Wang, Y.L., Frauwirth, K.A., Rangwala, S.M., Lazar, M.A. and Thompson, C.B. (2002) J. Biol. Chem. 277, 31781–31788.
[8] Brummelkamp, T.R., Bernards, R. and Agami, R. (2002) Science 296, 550–553.
[9] Abbas-Terki, T., Blanco-Bose, W., Deglon, N., Pralong, W. and Aebischer, P. (2002) Hum. Gene Ther. 13, 2197–2201.
[10] Hasuwa, H., Kaseda, K., Einarsdottir, T. and Okabe, M. (2002) FEBS Lett. 532, 227–230.
[11] Kunath, T., Gish, G., Lickert, H., Jones, N., Pawson, T. and Rossant, J. (2003) Nat. Biotechnol. 21, 559–561.
[12] Naldini, L., Blomer, U., Gallay, P., Ory, D., Mulligan, R., Gage, F.H., Verma, I.M. and Trono, D. (1996) Science 272, 263–267.
[13] Kafri, T., Blomer, U., Peterson, D.A., Gage, F.H. and Verma, I.M. (1997) Nat. Genet. 17, 314–317.
[14] Takahashi, M., Miyoshi, H., Verma, I.M. and Gage, F.H. (1999) J. Virol. 73, 7812–7816.
[15] Miyoshi, H., Smith, K.A., Mosier, D.E., Verma, I.M. and Torbett, B.E. (1999) Science 283, 682–686.
[16] Pfeifer, A., Kessler, T., Yang, M., Baranov, E., Kootstra, N., Cheresh, D.A., Hoffman, R.M. and Verma, I.M. (2001) Mol. Ther. 3, 319–322.
[17] Brummelkamp, T.R., Bernards, R. and Agami, R. (2002) Cancer Cell 2, 243–247.
[18] van de Wetering, M. et al. (2003) EMBO Rep. 4, 609–615.
[19] Mizuguchi, H. and Kay, M.A. (1999) Hum. Gene Ther. 10, 2013–2017.
[20] Tahara-Hanaoka, S., Sudo, K., Ema, H., Miyoshi, H. and Nakauchi, H. (2002) Exp. Hematol. 30, 11–17.
[21] Miyoshi, H., Blomer, U., Takahashi, M., Gage, F.H. and Verma, I.M. (1998) J. Virol. 72, 8150–8157.
[22] Tontonoz, P., Hu, E., Graves, R.A., Budavari, A.I. and Spiegelman, B.M. (1994) Genes Dev. 8, 1224–1234.
[23] Gimble, J.M., Robinson, C.E., Wu, X., Kelly, K.A., Rodriguez, B.R., Kliewer, S.A., Lehmann, J.M. and Morris, D.C. (1996) Mol. Pharmacol. 50, 1087–1094.
[24] Baer, M., Nilsen, T.W., Costigan, C. and Altman, S. (1990) Nucleic Acids Res. 18, 97–103.
[25] Chawla, A., Schwarz, E.J., Dimaculangan, D.D. and Lazar, M.A. (1994) Endocrinology 135, 798–800.
[26] Kliewer, S.A., Forman, B.M., Blumberg, B., Ong, E.S., Borgmeyer, U., Mangelsdorf, D.J., Umesono, K. and Evans, R.M. (1994) Proc. Natl. Acad. Sci. USA 91, 7355–7359.
[27] Tontonoz, P., Hu, E. and Spiegelman, B.M. (1994) Cell 79, 1147–1156.
[28] Ramirez-Zacarias, J.L., Castro-Munozledo, F. and Kuri-Harcuch, W. (1992) Histochemistry 97, 493–497.
[29] Green, H. and Kehinde, O. (1975) Cell 5, 19–27.
[30] Wise, L.S. and Green, H. (1979) J. Biol. Chem. 254, 273–275.
[31] Doench, J.G., Petersen, C.P. and Sharp, P.A. (2003) Genes Dev. 17, 438–442.

Available online at www.sciencedirect.com
SCIENCE DIRECT®
Biochemical and Biophysical Research Communications 323 (2004) 583–591
BBRC
www.elsevier.com/locate/ybbrc

Optimal construction of non-immune scFv phage display libraries from mouse bone marrow and spleen established to select specific scFvs efficiently binding to antigen

Takayuki Okamoto[a,1], Yohei Mukai[a,1], Yasuo Yoshioka[a,b,1], Hiroko Shibata[a], Maki Kawamura[a], Yoko Yamamoto[a], Shinsaku Nakagawa[a], Haruhiko Kamada[d], Takao Hayakawa[b], Tadanori Mayumi[c], Yasuo Tsutsumi[a,d,*]

[a] *Department of Biopharmaceutics, Graduate School of Pharmaceutical Sciences, Osaka University, 1-6 Yamadaoka, Suita, Osaka 565-0871, Japan*
[b] *National Institute of Health Sciences (NIHS), 1-18-1, Kamiyoga, Setagaya-ku, Tokyo 158-8501, Japan*
[c] *Department of Cell Therapeutics, Graduate School of Pharmaceutical Sciences, Kobe Gakuin University, 518 Arise, Ikawadani, Nishiku, Kobe 651-2180, Japan*
[d] *National Institute of Health Sciences, Osaka Branch Fundamental Research Laboratories for Development of Medicine, 7-6-8 Saito-Asagi, Ibaraki, Osaka 567-0085, Japan*

Received 20 May 2004

Abstract

Monoclonal antibodies (MAbs) are widely applied in basic research, medicine, and the pharmaceutical industry. Recently, applications and generations of MAbs have been increasingly attracting attention in many research areas since MAbs could be produced in large quantities with the development of genetic technology and antibody engineering. On the other hand, in recent years, phage display system has been developed for high-throughput isolation and generation of novel MAbs that have high affinity with various antigens. This technology is capable of constructing "Library" containing billions of phage repertoires displaying various antibody fragments, and rapid selection of a specific MAb from this phage library. Additionally, this technology has a great advantage that MAbs can be generated without immunization to animals. However, there are still relatively few reports confirming that useful MAbs can be derived from non-immune antibody libraries. The latter, as undertaken by current methods, seem unable to achieve the high quality required to produce useful MAbs for any desired antigen because cloning of antibody gene from non-immune donors is inefficient. This problem is caused by the fact that their RT-PCR primer sets, PCR conditions, and efficiency of subcloning through construction of antibody gene library cannot encompass all the antibody diversity. In an attempt to overcome some of these earlier problems, here we describe an optimized method to establish a high quality, non-immune library from mouse bone-marrow and spleen, and assess its diversity in terms of content of multiple antibodies for a wide antigenic repertoire. As an example of the application of the methodology, we describe the selection of specific MAbs binding to Luciferase and identify at least 18 different clones. Using this non-immune mouse antibody library, we also obtained MAbs for VEGF, VEGF receptor 2, TNF-α, and *Pseudomonas* Exotoxin, confirming the high quality of the library and its suitability for this application.

Keywords: Phage display system; Non-immune library; Antibody therapy

Monoclonal antibodies (MAbs) are essential tools in molecular biology, clinical examinations, medical treatment of cancer, infectious diseases, and in many other areas [1–3]. MAbs are routinely generated from mice

* Corresponding author. Fax: +81 6 6879 8178.
E-mail addresses: tsutsumi@phs.osaka-u.ac.jp, ytsutsumi@nihs.go.jp (Y. Tsutsumi).
[1] These authors contributed equally to the work.

0006-291X/$ - see front matter © 2004 Elsevier Inc. All rights reserved.
doi:10.1016/j.bbrc.2004.08.131

or rats using hybridoma technology [4,5], which involves immunizing the animal with a target antigen, isolating the relevant B cells, and fusing them with immortal cell lines to create antibody-producing hybridoma cells. Typically, in order to generate MAbs for a particular antigen, a number of mice are immunized over a period of 2–6 months, followed by a further 1–2 months of laboratory work before the hybridoma cells can be finally produced.

In contrast, the phage display system represents a more rapid technique, because it does not require immunizing the donor with antigen and avoids much laborious laboratory work. Using phage display system, various antibody fragments can be displayed on the surface of filamentous phages containing the antibody gene as a phagemid [6–9]. On the other hand, antibody fragments including scFv (single-chain fragment variable) molecules have been developed for potential clinical applications [10–12]. ScFvs, smallest antibody fragments, are composed of a light chain and a heavy chain variable region (VL and VH, respectively) joined via a short peptide spacer sequence. Thus, the phage display system has been developed from recombinant scFv techniques for the cloning and expression of cDNAs encoding the variable regions of antibody VL and VH chains and allows the in vitro generation of large antibody repertoires [13]. The processes required for this phage display system, i.e., RT-PCR, and PCR amplification and selection from phages displaying combinatorial libraries, constitute a selection step analogous to that occurring during the primary immune response. These processes allow the in vitro construction of antibody fragments of diverse specificities. The selection of non-immune libraries can yield a set of recombinant scFvs within 2–3 weeks. Moreover, a critical advantage of this technology is the direct link that exists between the experimental phenotype and its encapsulated genotype. This technology allows the evolution of the selected binders into optimized molecules, by affinity maturation via hot spot mutation [14,15] and enhancing in vivo stability by lowering the p*I* effect [16].

Use of such antibody libraries from non-immune donors has enabled the identification of MAbs in rapid high-throughput mode; however, successful initial construction of the non-immune libraries has thus far been achieved only by a small number of research groups [17,18]. In addition, non-immune libraries constructed by current methods lack the full variable region gene repertoire and show low efficiency of generation and creation of scFv gene diversity. In other words, previous methods for library construction are unable to encompass all potential antibody gene repertoires, because the primer set for cloning the VH and VL genes is not satisfactory. Additionally, PCR amplification conditions, efficiency of ligation of scFv gene to vector, and conditions employed for phage antibody secretion are all very important factors for establishing a large non-immune library. Establishing non-immune antibody libraries of high quality and great diversity under optimized conditions is needed.

In this study, we optimized the above-mentioned conditions to establish a high quality non-immune library, with a large size that potentially includes many specificities present in vivo. We describe the production of a mouse non-immune library based on optimized conditions including the nature of the primer sets for cloning antibody repertoires, PCR and ligation conditions, and phage production. By way of illustration, 18 specific monoclonal scFvs were selected from this library on the basis of binding to Luciferase, a model antigen. Detailed analysis of the anti-Luciferase scFvs confirmed their specificity and sequence. To demonstrate the general efficacy of our approach, we selected specific scFvs binding to diverse antigens, namely, vascular endothelial growth factor (VEGF), VEGF receptor 2 (VEGF-R2), tumor necrosis factor-alpha (TNF-α), and *Pseudomonas* Exotoxin (PE). This optimized methodology permits the construction of a high quality phage library easily and it can be applied to the development of phage display systems.

Materials and methods

Construction of non-immune mouse scFv phage libraries. Fig. 1 is a flow diagram that shows the construction of a non-immune mouse scFv phage library. Total RNA was prepared from spleen tissue and bone marrow of non-immunized 6-week-old male C57BL/6, Balb/c, and C3H mice. Mouse mRNA was purified using oligo(dT) columns (Amersham–Pharmacia Biotech, Uppsala, Sweden) and subsequently first strand cDNA was generated using Superscript II reverse transcriptase (Invitrogen, Carlsbad, CA). From each cDNA, heavy- and light-chain genes were amplified separately and recombined by three subsequent PCRs. In the first-step PCR, the heavy- and light-chains were amplified. The light chain 5′ primers were modified to include an *Sfi*I site, and heavy chain 3′ primers to include a *Not*I site. Light chain 3′ primers were designed to assemble with heavy chain 5′ primers (Tables 1 and 2). Heavy and light chain variable region genes were amplified by PCR containing 2 μL cDNA and 25 pmol of each 5′ and 3′ primer, using the Expand High Fidelity PCR system (Roche Diagnostics, Indianapolis, IN, USA). The samples were cycled 35 times at 96 °C for 60 s, 55 °C for 60 s, and 68 °C for 60 s. The samples were then purified from the agarose gel by GenElute MINUS EtBr Spin Columns (Sigma Chemical, St. Louis, MO). In the second-step PCR, heavy and light chains were assembled. The first-step PCR products of heavy and light chains were mixed, and the assembly PCR containing equal amounts of the products was cycled 20 times at 96 °C for 60 s, 63 °C for 60 s, and 68 °C for 60 s without primers. The samples were purified with QIAquick PCR Purification Kits (QIAGEN, Valencia, CA). The third-step PCR extended the second PCR products by overlap PCR. This PCR extends the scFv gene (second-PCR products) using the following primers: the Y15 primer (5′-gcc aag ctt tgg agc ctt ttt ttt gga gat ttt caa cgt gaa aaa att att att cgc aat tcc ttt agt tgt tcc ttt cta tgc ggc cca gcc ggc cat ggc c-3′) and the Y16 primer (5′-cgc cgg cgt cca cgc ggc cac ggc ata ggc cta ggc gac ctt ggc gca cgg cgt atc tga caa ctt tca aca aat cgt ttt gga gta tgt ctt tta agt aaa tg-3′). The modified 5′ primer and 3′ primer are were extended from the *Sfi*I

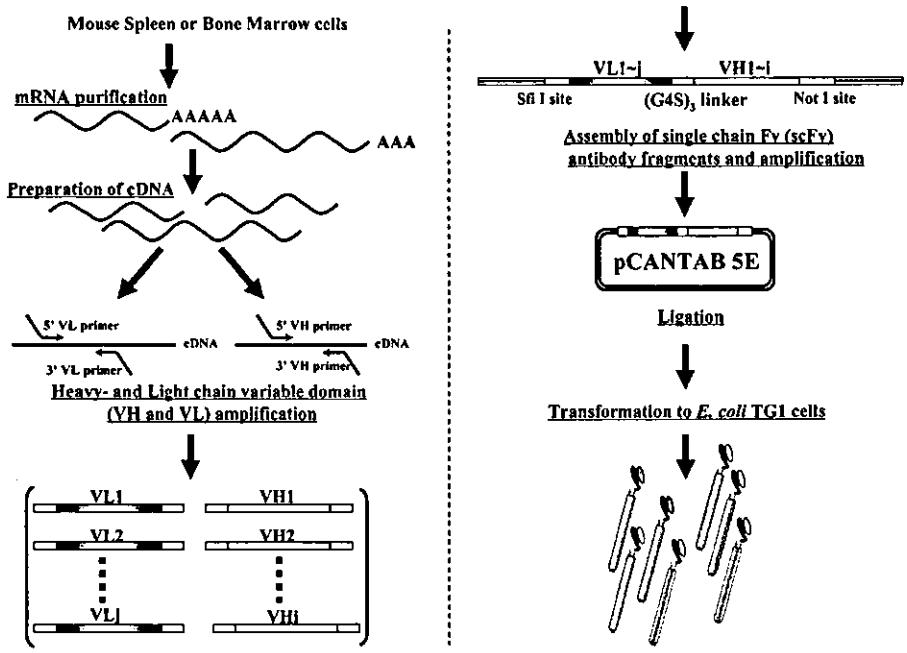

Fig. 1. Flow diagram illustrating construction of the scFv phage library.

Table 1
Primers for PCR amplification of mouse antibody light chain variable regions

VL-5′ primers	5′-cct ttc tat gcG GCC CAG CCG GCC atg gcc GAY ATT GTD HTV WCH CAG TC-3′
	5′-cct ttc tat gcG GCC CAG CCG GCC atg gcc GAY ATT NWK MTV AHD CAG TC-3′
	5′-cct ttc tat gcG GCC CAG CCG GCC atg gcc GAY RTY BWR MTS ACM CAR WC-3′
	5′-cct ttc tat gcG GCC CAG CCG GCC atg gcc GAY ATY SWG MTG ACN CAR BC-3′
	5′-cct ttc tat gcG GCC CAG CCG GCC atg gcc GAY RYT GTK RTR MYY MRG DW-3′
VL-3′ primers	5′-acc aga gcc gcc gcc gcc gct acc acc acc acc CCG TTY NAK YTC CAR CTT DG-3′
	5′-acc aga gcc gcc gcc gcc gct acc acc acc acc MCS TWB NAB HKY CAV YYT DG-3′

S = G/C, R = G/A, K = G/T, M = A/C, Y = C/T, W = A/T, H = A/C/T, B = C/G/T, V = A/C/G, D = A/G/T, and N = A/T/G/C.

Table 2
Primers for PCR amplification of mouse antibody heavy chain variable regions

VH-5′ primers	5′-agc ggc ggc ggc ggc tct ggt ggt ggt gga tcc SAK GTB MAG CTB MAG SAS TC-3′
	5′-agc ggc ggc ggc ggc tct ggt ggt ggt gga tcc SAG GTY CAR CTB CAR CAR TC-3′
	5′-agc ggc ggc ggc ggc tct ggt ggt ggt gga tcc SAV GTS MWS BTG RWG SAR TC-3′
	5′-agc ggc ggc ggc ggc tct ggt ggt ggt gga tcc GAK GTG MAV SKG RTG GAR TC-3′
	5′-agc ggc ggc ggc ggc tct ggt ggt ggt gga tcc GAR GTR MAR STT SWB GAG TC-3′
	5′-agc ggc ggc ggc ggc tct ggt ggt ggt gga tcc SAK GTB MMN YTV VWV SWR YS-3′
VH-3′ primers	5′-cgg cac cgg cgc acc tGC GGC CGC YGA RGA RAC DST GAS MRK RGT-3′
	5′-cgg cac cgg cgc acc tGC GGC CGC YGA RGA RRM SKK KAS WGW GRT-3′
	5′-cgg cac cgg cgc acc tGC GGC CGC YGA GGA GAC KGT GAS HGD GGH-3′

S = G/C, R = G/A, K = G/T, M = A/C, Y = C/T, W = A/T, H = A/C/T, B = C/G/T, V = A/C/G, D = A/G/T, N = A/T/G/C.

and *Not*I sites of scFv genes upstream by overlap PCR. The third overlap PCR was run under the same cycling conditions as the first-PCR at an annealing temperature of 65 °C.

Cloning of the mouse scFv repertoire into pCANTAB 5E. The PCR-amplified scFv DNAs and pCANTAB 5E phagemid vector were digested with *Not*I and *Sfi*I. The resulting scFv fragments were inserted into pCANTAB 5E phagemid vector to generate an scFv-gene III fusion library, using T4 ligase (Roche Diagnostics, Indianapolis, IN, USA) at 16 °C for 16 h. Ligated DNA populations were introduced into *Escherichia coli* (*E. coli*) TG1 using a Bio-Rad Gene Pulser (Bio-Rad Laboratories, CA). Each library was then grown by culturing at 37 °C in 2-YT medium, supplemented with ampicillin (100 μg/mL) and

glucose (2% w/v). Colonies were then collected, mixed with glycerol, and stored at −80 °C. Panning of phage particles was done as described earlier. Phage preparations were purified and concentrated by polyethylene glycol (PEG) precipitation.

Selection of anti-Luciferase antibodies. A large mouse scFv phage display library containing 5×10^8 clones was used for the selection. The library stock was grown in log phase, rescued with M13KO7 helper phage (Invitrogen, Carlsbad, CA), and amplified overnight in 2YTAK (2YT containing 100 μg/mL ampicillin and 50 μg/mL kanamycin) at 37 °C. The phage was precipitated with 4% PEG/0.5 M NaCl, resuspended in NTE buffer (100 mM NaCl, 10 mM Tris, and 1 mM EDTA) and incubated with 2% Block Ace at 4 °C for 1 h to block nonspecific binding. Immunotubes (Nunc maxisorp; Life Technologies, Merelbeke, Belgium) were coated with 10 μg/mL Luciferase (Promega, Madison, WI), TNF-α, VEGF-R2, VEGF or PE in carbonate/bicarbonate buffer (Sigma Chemical, St. Louis, MO). Prior to this, they were first blocked with 2% Block Ace at 4 °C for 1 h. Then the tubes were incubated with phage preparation at 4 °C for 1 h. After incubation, the tubes were washed 10 times with PBST (PBS containing 0.05% Tween 20) and subsequently with PBS. The bound phage was eluted at 4 °C for 10 min with 1 mL of freshly prepared 100 mM HCl solution. The eluted phage particles were incubated with 10 mL of log phase TG1 cells at 37 °C with shaking at 110 rpm for 20 min and at 250 rpm for 30 min. The infected cells were mixed with glycerol at −80 °C. For the next round of panning, 3 mL of infected TG1 cell stock was added to 50 mL of 2YTAG medium and grown to log phase. The culture was rescued with M13KO7 helper phage, amplified, precipitated, and used for selection, following the procedure described earlier. The panning process was repeated.

Phage ELISA. After the panning process, individual TG1 clones were picked, grown at 37 °C in 96-well plates, and rescued with M13KO7 helper phage as described earlier. The amplified phage preparation was blocked with 2% Block Ace at 4 °C for 1 h and then added to Maxi-sorp 96-well microtiter plates coated with Luciferase or ovalbumin (10 μg/mL, SIGMA). After overnight incubation at 4 °C, the plates were washed three times with PBST and PBS, and incubated with a mouse anti-M13 phage-horseradish peroxidase (HRP) conjugate (Amersham–Pharmacia Biotech, Uppsala, Sweden). The plates were washed three times, TMB peroxidase substrate was added, and the absorbance was read at 450 nm using a microplate reader (Bio-Rad Laboratories, CA).

DNA BstNI pattern analysis and nucleotide sequencing. After the third round of panning, the diversity of the selected scFv clones was analyzed by restriction enzyme digestion patterns (i.e., DNA fingerprint analysis). The scFv gene insert of individual clones was amplified by PCR using the following primers: pCANTAB5-S1 primer (5′-cag gaa aca gct atg ac-3′) and pCANTAB5-S6 primer (5′-gta aaa cga cga cgg cca gt-3′). The amplified product was digested with a frequent-cutting enzyme, *Bst*NI (NEB), and analyzed on agarose gels. DNA sequencing was performed using the BigDye Terminator Ready Reaction Kit (Applied Biosystems).

Results and discussion

In this study, we present the principle of selecting specific scFv for any antigen from a non-immune mouse scFv library (Fig. 1). For the construction of these large libraries, mRNA was extracted from mouse bone marrow and spleen cells, and the cDNA fragments encoding VL and VH genes were amplified by RT-PCR. In previous methods, the VL and VH genes were not adequately

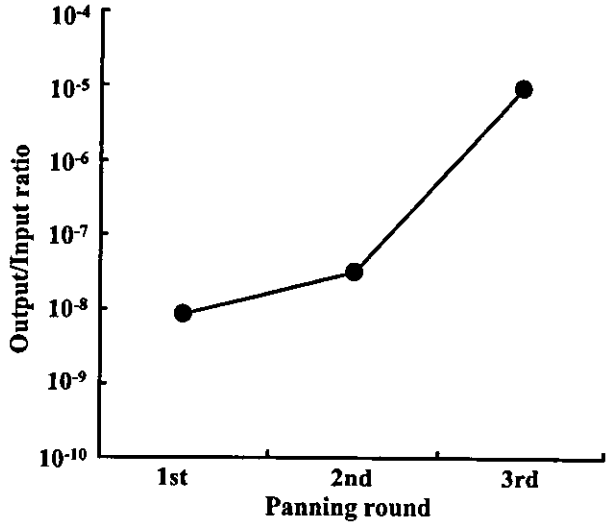

Fig. 3. Selection of phage-scFv libraries by panning in immunotubes. Luciferase-coated immunotubes were first blocked with 2% Block Ace at 4 °C for 1 h and then incubated with phage preparations at 37 °C for 1 h. The tubes were washed 10 times with PBST (PBS containing 0.05% Tween 20) followed by PBS. The bound phage was eluted with 1 mL of freshly prepared 100 mM HCl solution at 4 °C for 10 min. The ratio was calculated as follows: (output phage titer)/(input phage titer). The second and third panning input phage preparations were amplified from the last rounds of the output phages.

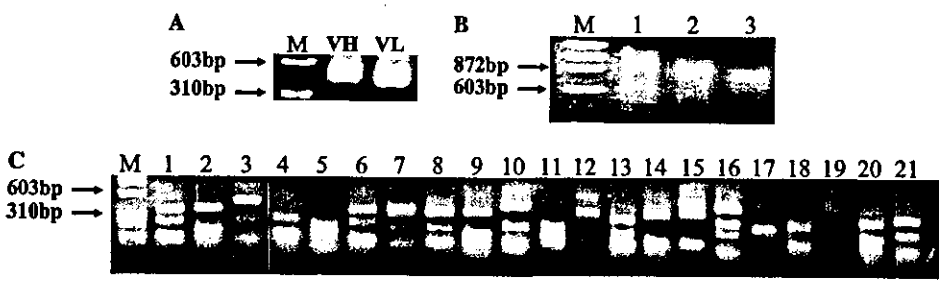

Fig. 2. Construction of non-immune mouse scFv library. (A) The amplified variable regions of heavy- and light-chains from mouse bone marrow and spleen. (B) Preparation of scFv genes. Lane 1, third PCR products; lane 2, scFv genes digested with *Sfi*I; and lane 3, scFv genes digested with *Not*I. (C) Non-immune scFv encoding inserts of 21 phage clones were amplified by PCR using pCANTAB5-S1 and pCANTAB5-S6 primers. The amplified products were digested with the frequent-cutting enzyme *Bst*NI at 60 °C for 2 h. The restriction patterns of samples were analyzed on agarose gels.